horticulturae

MDPI

Article

Elucidating Softening Mechanism of Honey Peach (*Prunus persica* L.) Stored at Ambient Temperature Using Untargeted Metabolomics Based on Liquid Chromatography-Mass Spectrometry

Xiaoxue Kong [1,2,†], Haibo Luo [2,†], Yanan Chen [2], Hui Shen [1], Pingping Shi [1], Fang Yang [1], Hong Li [3,*] and Lijuan Yu [1,*]

[1] Agro-Products Processing Research Institute, Yunnan Academy of Agricultural Sciences, Kunming 650221, China; 45225@njnu.edu.cn (X.K.); shenhui@yaas.org.cn (H.S.); spp@yaas.org.cn (P.S.); yf@yaas.org.cn (F.Y.)

[2] School of Food Science and Pharmaceutical Engineering, Nanjing Normal University, Nanjing 210023, China; 45235@njnu.edu.cn (H.L.); chenyn813@163.com (Y.C.)

[3] College of Food Science and Technology, Yunnan Agricultural University, Kunming 650201, China

* Correspondence: lihong@yaas.org.cn (H.L.); ylj@yaas.org.cn (L.Y.)

† These authors contributed equally to this work.

Abstract: Peach fruit softening is the result of a series of complex physiological and biochemical reactions that influence shelf life and consumer acceptance; however, the precise mechanisms underlying softening remain unclear. We conducted a metabolomic study of the flesh and peel of the honey peach (*Prunus persica* L.) to identify critical metabolites before and after fruit softening. Compared to the pre-softening profiles, 155 peel metabolites and 91 flesh metabolites exhibited significant changes after softening ($|\log_2(FC)| > 1$; $p < 0.05$). These metabolites were mainly associated with carbohydrate metabolism, respiratory chain and energy metabolism (citrate cycle, pantothenate and CoA biosynthesis, nicotinate and nicotinamide metabolism, and pentose and glucuronate interconversions), reactive oxygen species (ROS) metabolism, amino acid metabolism, and pyrimidine metabolism. During peach fruit softening, energy supply, carbohydrate and amino acid metabolism, oxidative damage, and plant hormone metabolism were enhanced, whereas amino acid biosynthesis and cell growth declined. These findings contribute to our understanding of the complex mechanisms of postharvest fruit softening, and may assist breeding programs in improving peach fruit quality during storage.

Keywords: honey peach; softening; untargeted metabolomics; LC–MS; metabolites

check for updates

Citation: Kong, X.; Luo, H.; Chen, Y.; Shen, H.; Shi, P.; Yang, F.; Li, H.; Yu, L. Elucidating Softening Mechanism of Honey Peach (*Prunus persica* L.) Stored at Ambient Temperature Using Untargeted Metabolomics Based on Liquid Chromatography-Mass Spectrometry. *Horticulturae* **2023**, *9*, 1210. https://doi.org/10.3390/horticulturae9111210

Academic Editors: Tao Luo, Zhenxian Wu and Xiaomeng Guo

Received: 2 October 2023
Revised: 31 October 2023
Accepted: 2 November 2023
Published: 8 November 2023

1. Introduction

Honey peach (*Prunus persica* L.; family *Rosaceae*) fruit is an important horticultural product cultured worldwide for its pleasant aroma, juicy texture, delicate flavor, and rich nutrient content [1]. Honey peaches are rich in phytochemicals, including lipids, vitamins, nucleotides, phenolics (phenolic acids and flavonoids), carotenoids, triterpenes, and alkaloids [2]. Many phytochemicals possess health-promoting benefits such as free radical neutralization, cancer prevention, and heart disease prevention [3]. However, honey peaches are climacteric fruits with a vigorous postharvest respiratory physiological metabolism. Honey peach softening refers to the transition of the fruit from a ripe stage to an overripe stage, where moderate softening is a sign of complete maturity. Many phytochemicals are formed during the softening process [4], although excessive softening leads to postharvest quality deterioration, storage and transportation limitations, and reduced shelf life and market value.

Fruit softening involves a series of complex physiological and metabolic processes. Fruit softening during storage is generally thought to be caused mainly by cell wall

structural alteration and degradation. Pectin, cellulose, hemicellulose, and other plant polysaccharides are the main components of most plant cell walls and play key roles in maintaining cell structure [5,6]. Comparative proteomics analysis of peaches at different ripening stages revealed that the differentially expressed proteins were mainly involved in cellular activities such as sugar metabolism, membrane structure, and cell-cycle control; in particular, polygalacturonase, pectate lyase, calmodulin, and calcineurin B-like protein exhibited functional roles in controlling fruit development and maintaining textural integrity during ripening [7–10]. In addition, several studies have found that plant hormone regulation, starch degradation, and energy metabolism are involved in fruit softening. Specifically, ethylene and abscisic acid play important regulatory roles in the final stage of peach ripening. Treatment with exogenous ethylene, which regulates respiration in climacteric fruit such as peaches, rapidly reduced fruit hardness, whereas 1-MCP treatment significantly delayed softening [11,12]. Abscisic acid is an important regulatory factor of fruit senescence after ripening, speeding up ripening and softening processes [13]. Amylase-catalyzed starch degradation increased the contents of soluble solids and reduced sugars, resulting in decreased fruit firmness [14,15]; therefore, postharvest starch degradation and sucrose metabolism may also contribute to peach softening. However, peach softening is a complex process, and its precise phytochemical variations and metabolic mechanism remain to be clarified.

Metabolomics is a powerful strategy for effectively identifying and quantifying metabolites within cells or tissues [16,17], providing an impartial approach for investigating correlations among interconnected metabolites via multiple pathways [18]. In recent years, metabolomics has been used to investigate the metabolic mechanisms underlying peach ripening and senescence [19]. The most commonly employed analytical techniques are liquid chromatography (LC)–tandem mass spectrometry (MS/MS) and nuclear magnetic resonance (NMR). Compared to NMR, LC-MS/MS offers superior resolution of chromatographic peaks, heightened sensitivity, and greater efficiency [20,21]. Untargeted metabolomics, a widely employed approach for qualitative sample analysis, can rapidly identify and classify metabolites based on differences in metabolic pathway maps, and based on LC-MS/MS, can reliably analyze metabolic profiles [22,23].

The objective of this study was to elucidate the softening mechanism of postharvest peaches. We performed global untargeted metabolomic profiling via LC-MS to study the mechanistic variation in peaches harvested at 90% maturity (pre-softening) and stored for 4 days at 25 ± 1 °C and 80–90% relative humidity (post-softening). We identified differential metabolites and analyzed the associated metabolic pathways. Our findings clarify the mechanism underlying peach softening, and support metabolic regulation to extend their shelf life, thereby reducing peach storage and transportation losses.

2. Materials and Methods

2.1. Analytical Standards and Reagents

Analytical standards were purchased from Thermo Fisher Scientific (Waltham, MA, USA), including methanol (≥99%; CAS no.: 67-56-1), acetonitrile (≥99%; CAS no.: 75-05-9), and formic acid (LC-MS grade; CAS no.: 64-18-6). The major reagents were purchased from Nanjing Jiancheng Bioengineering Institute (Nanjing, China), including dihydrogen phosphate potassium (≥99%; CAS no.: 7778-77-0), dipotassium hydrogen phosphate (≥99%; CAS no.: 7758-11-4), and L-2-chlorobenzalanine (≥98.5%; CAS no.: 103616-89-3).

2.2. Plant Materials and Treatments

Fresh peaches were hand-harvested from a *Prunus persica* L. orchard in Laishan, Shandong Province, China. All samples were similar in size and color, and lacking visible defects. To investigate the softening mechanism, samples were stored at 25 ± 1 °C and relative humidity of 80–90% for 4 days; hard peaches from the day of harvest (day 0) were used as the control.

The peel and flesh of hard peaches (PHP and FHP, respectively) and stored peaches (PSP and FSP, respectively) were sampled using a sharp stainless steel knife, cut into small pieces (3–5 mm^3), frozen with liquid nitrogen, and stored at −80 °C until analysis.

2.3. Visualization of the Ultrastructure

The cell ultrastructure of peach peel and flesh were visualized as previously described by Luo et al. (2019), with some modifications [24]. Tissue blocks of approximately 1 mm^3 were sliced from peach surface and washed three times with cold phosphate-buffered saline (PBS, pH7.0, 0.1 M) for 15 min each. The samples were soaked in 2.5% (*w*/*v*) glutaraldehyde for 24 h at 4 °C, washed with PBS three times, and then soaked in 1% osmic acid fixative solution for 2 h. The samples were washed with PBS (pH7.4) three times, and dehydrated in 50%, 70%, and 90% ethanol for 15 min each, followed by 100% ethanol for 20 min. After fixing with conductive carbon adhesive and spray gold with an ion sputtering instrument for 50 s, and the slices were observed under a FEI Nova Nano 450 scanning electron microscope (FEI Company, Hillsboro, OR, USA).

2.4. Sample Preparation for LC-MS

For each sample, 80 mg was transferred to a 1.5-mL Eppendorf tube containing two small steel balls. Then, 1 mL of a methanol and water mixture (7:3, *v*/*v*) was added and the tube was placed in a −20 °C freezer for 2 min. Next, the sample was ground at 60 Hz for 2 min, vortexed, and ultrasonicated at ambient temperature for 30 min. The tube was then stored at −20 °C for 12 h before centrifugation for 10 min (10,000× *g*, 4 °C). From each sample tube, 150 μL of supernatant was filtered through a 0.22 μm organic-phase pinhole filter and transferred to an LC vial, which was stored at −80 °C until LC-MS analysis.

To avoid instrument errors, quality control (QC) samples were prepared by mixing all samples in equal volumes and analyzed to test the stability of the instrument system and the repeatability of sampling.

2.5. Ultra-High-Performance LC with Quadrupole Time-of-Flight Mass Spectrometry (UPLC-Q-TOF-MS)

UPLC-Q-TOF-MS analysis was performed using a Nexera UHPLC (Shimadzu, Kyoto, Japan) combined with a Q-Exactive high-resolution MS (Thermo Fisher Scientific). Samples were separated with an ACQUITY UPLC HSS T3 column (100 mm × 2.1 mm, 1.8 μm; Waters Corp., Milford, MA, USA) following the manufacturer's procedure. The binary gradient elution system consisted of (A) water containing 0.1% formic acid and (B) acetonitrile containing 0.1% formic acid. The injection volume was 2 μL, the column temperature was 45 °C, and the flow rate was 0.35 mL min^{-1}. The separation gradient was as follows: 0 min, 5% B; 4 min, 30% B; 8 min, 50% B; 10 min, 80% B; 14 min, 100% B; 15.1 min, 5% B; and 16 min, 5% B.

Mass spectrometric data were acquired with a Q-Exactive Plus MS (Thermo Fisher Scientific, Waltham, MA, USA) with an electrospray ionization source. The MS parameters were as follows: source spray voltage of 3.00 kV in the negative and 3.50 kV in the positive ion mode, and capillary temperature of 320 °C. All data were collected in MS^E mode, with a scan range of 100–1200, a full scan at a resolution of 70,000, and a normalized collision energy of 30 eV. Data were collected in data-dependent acquisition or MS/MS mode again to obtain more fragment ions and detailed information pertaining to metabolites.

2.6. Metabolome Data Analysis

The Progenesis QI v2.3 software (Nonlinear Dynamics, Newcastle, UK) was employed for baseline filtering, retention time correction, peak identification and alignment, and peak area normalization. The main parameters were a precursor tolerance of 5 mg L^{-1}, product tolerance of 10 mg L^{-1}, and production threshold of 5%. Compounds were identified based on their mass-to-charge ratio (*m*/*z*), secondary fragments, and isotopic distribution using the plant metabolome database. Each analysis was performed six times and pre-processed

by subtracting the blank response and aligning according to the QC sample. Ion peaks with all missing values (0 value) > 50% in the group were deleted. Compounds obtained qualitatively were screened according to their qualitative result scores; those with scores below 36 (out of 60) were regarded as inaccurate and deleted.

For multivariate statistical analysis, normalized data were imported into SIMCA-P v13.0 (Umetrics AB, Umea, Sweden). The processed data were analyzed using principal component analysis (PCA) to observe the overall distribution among the samples and the stability of the whole analysis methodology. Orthogonal partial least-squares discriminant analysis (OPLS-DA) was used to distinguish metabolites that differed between the pre- and post-softening groups. To prevent overfitting, seven-fold cross-validation and 200-response permutation testing were performed to evaluate model quality. Univariate statistics mainly included Student's *t*-test and fold change (FC) analysis to compare metabolites between two groups. Differential metabolites between the pre- and post-softening groups were selected based on a variable importance of projection (VIP) score > 1, $p < 0.05$, and m (i.e., $|\log_2(FC)| > 1$) [25].

Differential metabolites identified using LC-MS and associated with diverse pathways were visualized by plotting a heatmap (http://www.r-project.org, accessed on 26 May 2023) and analyzed via metabolomics pathway analysis (http://www.metaboanalyst.ca/, accessed on 27 May 2023). The Kyoto Encyclopedia of Genes and Genomes (KEGG) database (http://www.kegg.jp/, accessed on 27 May 2023) was used to determine the position and function of each metabolite in various metabolic pathways.

3. Results

3.1. Cellular Ultrastructure of Peaches before and after Softening

The morphologies of peach peel and flesh before softening (day 0; the day of harvesting) and after softening (day 4 of storage at 25 °C) were observed using scanning electron microscopy. Before softening, the fruit cells were compact, full, uniform in size, and closely arranged, and the cell edges were clearly visible (Figure 1A). After softening, the intercellular space increased, the edges of some cells became obscured with no evident boundary, and there were different degrees of contractions and folds, indicating that the cell structure of the fruit was damaged to an extent (Figure 1B).

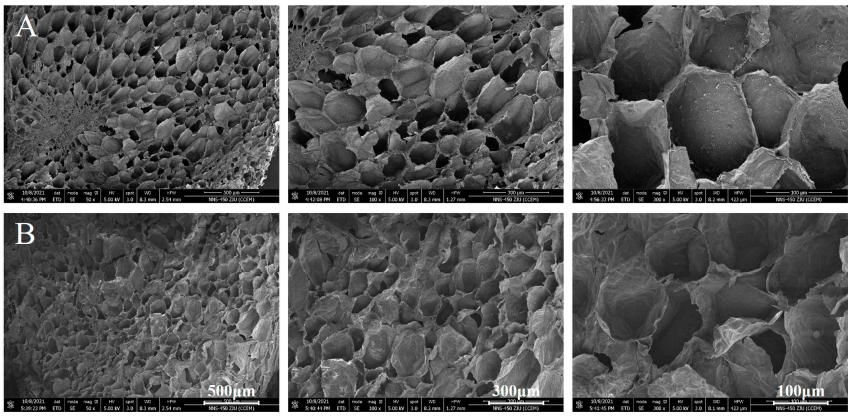

Figure 1. The cell ultrastructure of peach fruit before (**A**) and after (**B**) softening.

3.2. Metabolite Identification

The five sample groups (QC, PSP, FSP, PHP, and FHP) were analyzed using UPLC-Q-TOF-MS. In total, 7778 and 5577 precursor molecules were extracted in positive and negative ion modes, respectively. Progenesis QI v2.3 software was applied to process the raw UPLC-Q-TOF-MS data. Ultimately, 1660 metabolite ion features were detected. Detailed information regarding the metabolites, including pathway analysis, chemical analysis, m/z values, retention time, exact mass, molecular formula, mass error, precursor type, CAS number, and KEGG code, are presented in Table S1.

3.3. QC and Identification of Differential Metabolites

PCA, an unsupervised multivariate analysis, was performed to evaluate the stability of the system. In the score plots in Figure 2A, which were obtained from seven-fold cross-validation, the QC samples were clustered together, indicating satisfactory stability and reproducibility of the UPLC-Q-TOF-MS method. The six replicates of each group were clearly separated. The first two PCs explained 59.6% and 20.2% of the total variance, respectively. To more intuitively display the relationship between the QC samples and other samples, we conducted hierarchical clustering of the expression levels of all metabolites (Figure 2B).

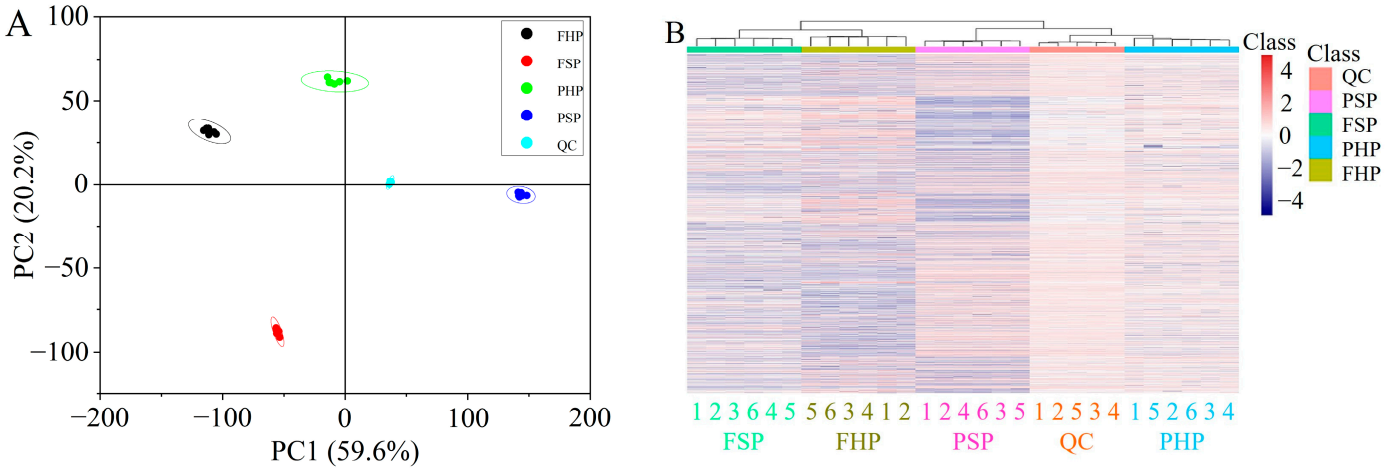

Figure 2. PCA score chart (**A**) and heatmap (**B**) of all samples.

To further confirm the differential metabolites between pre- and post-softening of peach peel (PSP/PHP) and flesh (FSP/FHP) samples, and filter out irrelevant components, OPLS-DA was used to maximize the differences between the groups PSP/PHP and FSP/FHP (Figure 3). Parameter values (R^2X, R^2Y, and Q^2) closer to 1 indicated a more stable and reliable model; the values for the PSP/PHP and FSP/FHP models were 0.967 and 0.965 for R^2X, 1 and 0.999 for Q^2, and 1 and 1 for R^2Y. These results indicated that the mathematical models showed high predictive accuracy, and could be used to identify differential metabolites.

The following criteria were applied to identify significantly differential metabolites using the criteria VIP > 1, $p < 0.05$, and $|\log_2(FC)| > 1$. In total, 155 metabolites were selected in the groups PSP/PHP (81 upregulated, 74 downregulated), and 93 metabolites were selected in the groups FSP/FHP (50 upregulated, 43 downregulated). The numbers of differential metabolites are shown in Figure 4. Differential metabolites were visualized using volcano plots, with red and blue dots representing significantly up- and downregulated metabolites, respectively, and gray dots representing metabolites without significant changes (Figure 4). During the peach softening process, there were significant differences in metabolites in both peel and flesh, with only a few metabolites remaining unchanged. The identified metabolites were classified into 11 super-classes according to their KEGG annotations. The distribution is shown in Figures 5 and S1, and the differential metabolites in peaches before and after softening are listed in Table 1.

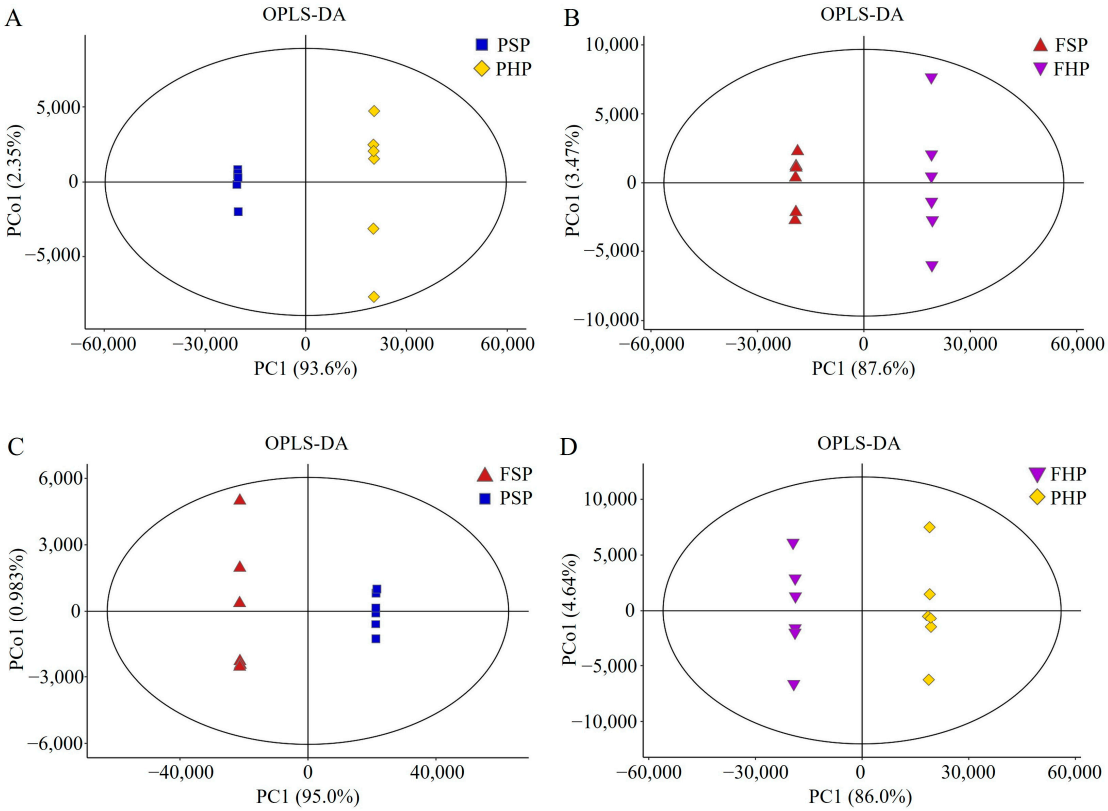

Figure 3. OPLS-DA score chart of PSP + PHP (**A**) and FSP + FHP (**B**). (**C**) FSP + PSP and (**D**) FHP + PHP.

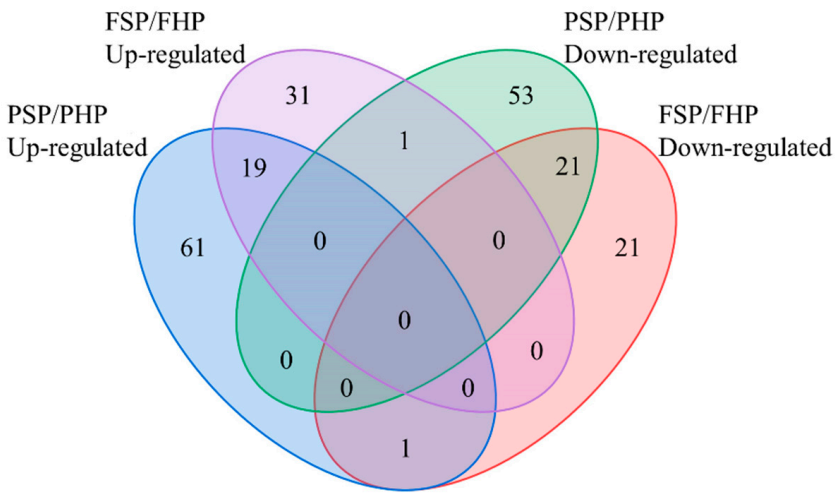

Figure 4. Number of differential metabolites in peach fruit before and after softening.

3.4. Hierarchical Clustering Analysis (HCA)

To directly evaluate differences in metabolite expression between the groups, we conducted HCA of the top 40 differential metabolites (Figure 6). Most were lipids and lipid-like molecules. In PSP/PHP, lipid-like molecules accounted for 35.9% of differential metabolites, and included the upregulated priverogenin B (|$\log_2$(FC)|: 37.26), goyaglycoside f (15.04), and lucidumol A (8.92) and the downregulated pitheduloside B (5.08), zedoarol (3.12), and angelic acid (2.02). In FSP/FHP, lipid-like molecules accounted for 34.04% of differential metabolites, and included the upregulated 10′-apo-beta-caroten-10′-al (|$\log_2$(FC)|: 35.19), corchorifatty acid F (4.50), and tragopogonsaponin B (3.77) and the downregulated goshon-

oside F3 (35.34), 3-O-cis-coumaroylmaslinic acid (4.49), and deoxynivalenol 3-glucoside (3.90). In addition, orotidine content was upregulated in both PSP/PHP (|$\log_2$(FC)|: 36.14) and FSP/FHP (36.16). Glutathione (GSH; |$\log_2$(FC)|: 37.25), uridine diphosphate-D-xylose (UDP-D-xylose; 35.86), N-gamma-L-glutamyl-D-alanine (35.16), procyanidin B1 (9.52), and procyanidin B2 (8.67) increased significantly only in FSP/FHP. Overall, these differential metabolites were related to changes in cell membrane lipid oxidation, energy production, pectin biosynthesis, characteristic volatile components, and color.

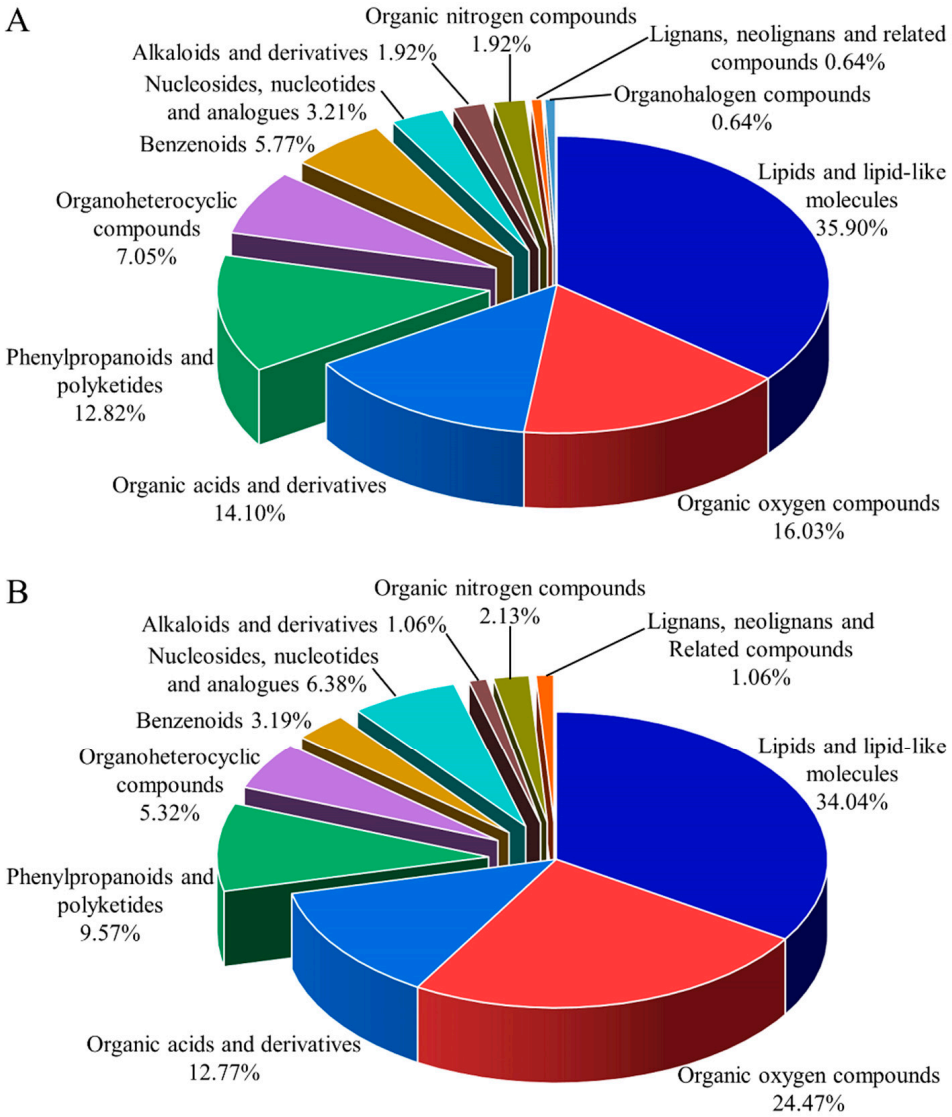

Figure 5. The super class distribution of identified differential metabolites covering 11 groups categorized according to their molecular structure. (**A**) PSP/PHP; (**B**) FSP/FHP.

Table 1. The differential metabolites in peach fruit before and after softening.

No.	ID	*m/z*	Retention Time (min)	Ion Mode	Metabolites	Compound ID	PSP/PHP	FSP/FHP
Alkaloids and derivatives								
1	5.03_553.2138m/z	553.2138	5.0349167	neg	Dehydroaporheine	HMDB0033355	5.5528348	
2	0.91_675.0976m/z	675.09764	0.9134167	neg	Prebetanin	HMDB0029411	−1.1931527	−0.2097159
3	0.82_137.0476n	160.0368	0.8212167	pos	Trigonelline	HMDB0000875	−6.296828	−3.4098136

Table 1. *Cont.*

No.	ID	*m/z*	Retention Time (min)	Ion Mode	Metabolites	Compound ID	PSP/PHP	FSP/FHP
Benzenoids								
4	12.05_333.1354m/z	333.13543	12.045667	neg	4′-Methoxymucidin	HMDB0030019	3.3352022	
5	12.59_501.2238m/z	501.2238	12.591167	neg	Purothionin AII	HMDB0039001	2.8072538	
6	10.98_292.2037n	293.21085	10.978267	pos	[7]-Paradol	HMDB0040806	2.5051899	
7	5.16_437.2030m/z	437.20305	5.15925	neg	N-Phenyl-2-naphthylamine	HMDB0032865	2.0844425	2.2331908
8	5.03_524.1345m/z	524.13452	5.0319	pos	Protohypericin	HMDB0034180	−1.2897264	
9	15.27_150.1277m/z	150.12768	15.2738	pos	p-Mentha-1,3,5,8-tetraene	HMDB0029641	−1.422287	−0.6103573
10	0.91_521.1087m/z	521.10873	0.9064	pos	Isomelitric acid A	HMDB0039523	−1.580731	−0.6180271
11	4.72_493.1289m/z	493.12889	4.7210667	pos	Palmidin A	HMDB0034038	−1.5901031	−1.6091476
12	1.83_278.1516n	301.14084	1.83035	pos	Dibutyl phthalate	HMDB0033244	−1.5974966	−0.7392945
13	4.72_583.1255m/z	583.12551	4.7247833	neg	Rheidin C	HMDB0038508		−1.2387168
Lignans, neolignans, and related compounds								
14	5.39_522.2105n	567.20854	5.3948167	neg	Isolariciresinol 4′-O-beta-D-glucoside	HMDB0040471	1.220256	
15	5.18_567.2084m/z	567.20838	5.1766	neg	Isolariciresinol 9-O-beta-D-glucoside	HMDB0032907	0.793055	−1.1147439
Lipids and lipid-like molecules								
16	15.26_474.3706n	497.35981	15.256067	pos	Priverogenin B	HMDB0034644	37.261839	
17	12.40_781.4695m/z	781.46946	12.4023	pos	Goyaglycoside f	HMDB0037124	15.036405	
18	15.10_472.3550n	495.34426	15.096133	pos	Lucidumol A	HMDB0033233	8.9189368	
19	14.51_446.3394n	469.32866	14.510817	pos	Secasterone	HMDB0040999	5.2741667	
20	15.13_448.3551n	471.3443	15.131617	pos	6-Deoxodolichosterone	HMDB0034332	5.1783877	
21	14.07_643.4173m/z	643.41728	14.06755	pos	Fasciculic acid A	HMDB0036439	3.6356945	
22	13.89_585.3757m/z	585.3757	13.894517	pos	Ganoderic acid Mg	HMDB0035999	2.9360617	
23	5.31_192.1514n	175.14811	5.3125	pos	gamma-Ionone	HMDB0034979	2.7246443	2.3180287
24	8.73_518.3244n	563.32257	8.7302167	neg	Ganolucidic acid C	HMDB0039691	2.462305	
25	14.21_508.3764n	531.36563	14.208733	pos	Fasciculol C	HMDB0035853	2.2688443	
26	9.66_535.2879m/z	535.28789	9.6555167	pos	Corchoroside A	HMDB0033846	2.0353167	
27	11.96_633.3968m/z	633.39684	11.955867	pos	Calenduloside E	HMDB0040851	1.9493374	
28	8.28_518.3234n	563.32252	8.2771333	neg	Ganoderic acid C2	HMDB0035304	1.9198447	
29	5.16_415.1936m/z	415.19356	5.1589	pos	S-Furanopetasitin	HMDB0036131	1.852255	1.1850532
30	5.50_415.1975m/z	415.1975	5.5021833	neg	(3S,7E,9S)-9-Hydroxy-4,7-megastigmadien-3-one 9-glucoside	HMDB0036822	1.7683917	1.4457104
31	5.29_377.1817m/z	377.18167	5.2873333	neg	6Z-8-Hydroxygeraniol 8-O-glucoside	HMDB0035025	1.7644214	1.3697986
32	5.58_373.1868m/z	373.1868	5.5755667	neg	6-Epi-7-isocucurbic acid glucoside	HMDB0029782	1.755631	
33	4.74_379.1610m/z	379.161	4.7429333	neg	Prenyl arabinosyl-(1->6)-glucoside	HMDB0041360	1.6820333	
34	5.47_282.1467n	281.13938	5.4670833	neg	Epidihydrophaseic acid	HMDB0038661	1.6585013	2.5180264
35	11.35_294.2193n	295.22654	11.354317	pos	2-Hydroxylinolenic acid	HMDB0031103	1.6570269	−1.0014807
36	9.15_502.3297n	547.32789	9.1458	neg	Ganolucidic acid B	HMDB0035751	1.6085416	
37	5.41_441.1978m/z	441.1978	5.4130167	neg	1-Hexanol arabinosylglucoside	HMDB0031689	1.6013305	
38	5.36_471.1872m/z	471.18718	5.35895	neg	11,13-Dihydrotaraxinic acid glucosyl ester	HMDB0035867	1.5551523	1.0746529
39	8.75_500.3135n	483.3102	8.7520667	pos	Ganolucidic acid A	HMDB0035302	1.5458326	
40	7.71_695.4014m/z	695.40141	7.7110833	neg	Momordicoside E	HMDB0035697	1.531432	
41	5.36_433.2079m/z	433.20795	5.35895	neg	Dihydroroseoside	HMDB0040614	1.4165233	
42	9.55_502.3292n	503.33642	9.5534167	pos	Medicagenic acid	HMDB0034551	1.3474913	
43	5.39_194.1670n	177.16372	5.3880333	pos	5-Isopropyl-2-(2-methylpropyl)-2-cyclohexen-1-one	HMDB0038216	1.3416272	
44	9.57_410.3181n	433.30983	9.5741	pos	(6alpha,22E)-6-Hydroxy-4,7,22-ergostatrien-3-one	HMDB0037380	1.3000743	
45	5.02_433.2080m/z	433.20803	5.0172833	neg	9,13-Dihydroxy-4-megastigmen-3-one 9-glucoside	HMDB0036318	1.2650463	
46	5.34_393.1768m/z	393.17677	5.3405333	neg	Nepetariaside	HMDB0039014	1.2443563	0.5806051

Table 1. *Cont.*

No.	ID	*m/z*	Retention Time (min)	Ion Mode	Metabolites	Compound ID	PSP/PHP	FSP/FHP
47	4.12_451.2187m/z	451.21868	4.12275	neg	Kiwiionoside	HMDB0038691	1.2365472	
48	5.09_427.1938m/z	427.19381	5.0859667	pos	Pisumionoside	HMDB0039947	1.2300592	
49	4.91_282.1466n	281.13946	4.9062833	neg	Pisumic acid	HMDB0039241	1.1927666	2.1976093
50	5.29_332.1832n	355.17243	5.2941167	pos	(2E,4E,7R)-2,7-Dimethyl-2,4-octadiene-1,8-diol 8-O-b-D-glucopyranoside	HMDB0038747	1.16536	0.727943
51	5.19_439.1822m/z	439.18219	5.1942167	neg	cis-3-Hexenyl b-primeveroside	HMDB0031690	1.1648099	
52	4.85_386.1940n	431.19223	4.8532667	neg	Citroside A	HMDB0030370	1.1464168	0.5008677
53	9.57_468.3237n	469.33097	9.5741	pos	Uralenolide	HMDB0038797	1.1359664	
54	9.15_502.3291n	503.33641	9.14545	pos	Esculentic acid (Phytolacca)	HMDB0034639	1.119195	
55	5.03_348.1781n	371.16731	5.0319	pos	Foeniculoside V	HMDB0034874	1.1036398	2.628105
56	5.95_421.2081m/z	421.20813	5.94505	neg	1-Octen-3-yl primeveroside	HMDB0032960	1.0953733	2.8884386
57	4.80_433.2080m/z	433.20798	4.7979	neg	Icariside B8	HMDB0036846	1.0514936	
58	5.48_280.1311n	279.1238	5.4847667	neg	Nigellic acid	HMDB0036094	1.0289409	1.9319225
59	10.99_679.3853m/z	679.38531	10.9895	neg	2alpha-Hydroxypyracrenic acid	HMDB0029780	1.0173618	
60	4.91_264.1360n	265.14329	4.90995	pos	3-Epiarmefolin	HMDB0036135	0.6841163	1.4082933
61	11.35_454.3443n	455.35163	11.354317	pos	Ursonic acid	HMDB0036007	−0.4947675	−1.8832459
62	5.57_458.1786n	481.16784	5.56605	pos	Deoxynivalenol 3-glucoside	HMDB0039852	−0.5041028	−3.9033631
63	11.34_473.3624m/z	473.36241	11.336667	pos	27-Hydroxyisomangiferolic acid	HMDB0036064	−0.6364165	−1.9997725
64	0.81_344.1316n	389.12984	0.81115	neg	Lactitol	HMDB0040937	−0.8733643	−1.2932778
65	12.98_438.3496n	439.35686	12.97695	pos	Thujyl 19-trachylobanoate	HMDB0036840	−0.9976602	−2.3387444
66	0.79_207.0503m/z	207.05031	0.7941333	neg	3-Hydroxymethylglutaric acid	HMDB0000355	−1.032756	−0.6809323
67	2.14_346.1261n	369.11535	2.1447	pos	Aucubin	HMDB0036562	−1.057286	−2.7078305
68	12.99_457.3672m/z	457.36724	12.99425	pos	beta-Elemolic acid	HMDB0034961	−1.2980053	−3.2925127
69	13.01_410.3545n	411.36175	13.011333	pos	Delta 8,14 -Sterol	HMDB0006928	−1.3317368	−2.134609
70	6.98_292.1883n	315.17763	6.9816333	pos	(S)-3-Octanol glucoside	HMDB0032958	−1.3828306	−0.5888407
71	11.39_277.1797m/z	277.1797	11.38935	pos	Phytuberin	HMDB0035754	−1.4766195	−0.5807962
72	14.14_310.3102m/z	310.31019	14.137933	pos	Geranylcitronellol	HMDB0032147	−1.5039805	
73	1.13_118.0865m/z	118.08646	1.1279	pos	Angelic acid	HMDB0029608	−2.0222781	−0.4844698
74	7.07_414.2252n	437.21441	7.0656833	pos	(4R,5S,7R,11S)-11,12-Dihydroxy-1(10)-spirovetiven-2-one 11-glucoside	HMDB0033150	−2.3741167	−0.7120234
75	6.47_264.1362n	263.12892	6.4695167	neg	Alkhanin	HMDB0036202	−2.8303188	
76	6.48_246.1255n	247.13273	6.4793333	pos	Zedoarol	HMDB0038202	−3.1160144	−1.5618091
77	13.03_883.5013m/z	883.50126	13.028717	pos	Pitheduloside B	HMDB0034865	−5.0778196	
78	14.99_377.2835m/z	377.2835	14.989867	pos	10′-Apo-beta-caroten-10′-al	HMDB0036887		35.192181
79	7.28_327.2176m/z	327.21764	7.2776667	neg	Corchorifatty acid F	HMDB0035919		4.5032417
80	4.54_926.4697n	927.47698	4.54215	pos	Tragopogonsaponin B	HMDB0037911		3.7664956
81	14.81_395.3670m/z	395.36697	14.812417	pos	Stigmasterol	HMDB0000937		3.149023
82	6.00_280.1311n	279.12379	6.00005	neg	13-Hydroxyabscisic acid	HMDB0036095		3.0563838
83	7.73_329.2334m/z	329.23337	7.7299667	neg	9,10,13-TriHOME	HMDB0004710		2.4227629
84	5.95_197.1536m/z	197.15357	5.9453333	pos	alpha-Terpineol acetate	HMDB0032051		1.9997694
85	5.48_280.1311n	279.1238	5.4847667	neg	Nigellic acid	HMDB0036094		1.932
86	5.49_280.1309n	263.12764	5.4853167	pos	Crispolide	HMDB0036695		1.3681446
87	12.19_618.3915n	619.39874	12.190483	pos	3-O-cis-Coumaroylmaslinic acid	HMDB0034539		−4.4936192
88	8.41_644.3399n	667.32928	8.40645	pos	Goshonoside F3	HMDB0038376		−35.34355

Table 1. *Cont.*

No.	ID	*m/z*	Retention Time (min)	Ion Mode	Metabolites	Compound ID	PSP/PHP	FSP/FHP
Nucleosides, nucleotides, and analogues								
89	0.79_575.1100m/z	575.10997	0.7941333	neg	Orotidine	HMDB0000788	36.14114	36.162397
90	5.58_485.1643m/z	485.16426	5.5755667	neg	Cytidine	HMDB0000089	1.7393751	
91	0.84_244.0926m/z	244.09257	0.8382333	pos	Cytarabine	HMDB0015122	1.3531597	
92	1.19_244.0693n	243.06197	1.1876833	neg	Pseudouridine	HMDB0000767	1.3475125	2.4172629
93	1.98_267.0722m/z	267.07222	1.9836833	neg	Inosine	HMDB0000195	−1.5091056	
94	0.81_535.0369m/z	535.0369	0.81115	neg	UDP-D-Xylose	HMDB0001018		35.862012
95	0.82_405.0089m/z	405.0089	0.8212167	pos	Uridine 5′-diphosphate	HMDB0000295		2.3748643
96	0.81_565.0474m/z	565.04744	0.81115	neg	Uridine diphosphate glucose	HMDB0000286		1.8838349
97	2.16_283.0915n	284.09878	2.1632167	pos	Guanosine	HMDB0000133		1.0393267
Organic acids and derivatives								
98	5.59_627.2407m/z	627.24074	5.5859833	pos	6-Hydroxysandoricin	HMDB0037556	1.1439601	
99	0.75_104.0710m/z	104.07099	0.7531167	pos	gamma-Aminobutyric acid	HMDB0000112	1.022634	1.8454808
100	1.12_192.0261n	191.01882	1.1193833	neg	Isocitric acid	HMDB0000193	−0.6188259	−1.6664215
101	1.13_147.0896n	130.0863	1.1279	pos	(2R,3R,4R)-2-Amino-4-hydroxy-3-methylpentanoic acid	HMDB0029449	−1.0198727	
102	1.11_146.0216n	129.0183	1.1108833	pos	Oxoglutaric acid	HMDB0000208	−1.1202847	−2.1185923
103	1.11_192.0271n	215.01603	1.1108833	pos	Citric acid	HMDB0000094	−1.1723789	−2.4103012
104	0.92_324.2166m/z	324.21664	0.9234167	pos	N-Jasmonoylisoleucine	HMDB0029391	−1.2033973	−0.5569567
105	1.98_141.0182m/z	141.01819	1.9789	pos	2-Methylene-4-oxopentanedioic acid	HMDB0037759	−1.4134892	−0.5977763
106	0.74_147.0763m/z	147.07632	0.7360833	pos	L-Glutamine	HMDB0000641	−1.4326922	
107	15.27_115.0505m/z	115.05045	15.2738	pos	Ureidopropionic acid	HMDB0000026	−1.4409771	−0.6352039
108	0.55_143.0339m/z	143.03386	0.5475833	pos	2-Methyl-4-oxopentanedioic acid	HMDB0039447	−1.4770497	−0.4252457
109	1.11_143.0339m/z	143.03388	1.1108833	pos	Oxoadipic acid	HMDB0000225	−1.5351415	−0.717166
110	4.18_202.0441m/z	202.0441	4.1786667	pos	L-Oxalylalbizziine	HMDB0039164	−1.6272134	−1.0362134
111	0.75_130.0500m/z	130.04995	0.7531167	pos	Pyroglutamic acid	HMDB0000267	−1.6855014	0.2421316
112	0.70_175.1189m/z	175.11886	0.7020333	pos	L-Arginine	HMDB0000517	−1.7061716	−1.3389484
113	0.72_134.0447m/z	134.04468	0.7190667	pos	L-Aspartic acid	HMDB0000191	−1.7547972	−0.9691886
114	2.84_166.0862m/z	166.08623	2.8391	pos	L-Phenylalanine	HMDB0000159	−1.8175168	−1.0099049
115	0.75_119.0586n	120.06569	0.7531167	pos	L-Threonine	HMDB0000167	−1.8452429	
116	0.89_118.0864m/z	118.08643	0.88935	pos	L-Valine	HMDB0000883	−1.9042841	−0.2565016
117	2.07_132.1020m/z	132.10196	2.0707667	pos	L-Isoleucine	HMDB0000172	−1.9205672	−1.2438406
118	0.84_116.0708m/z	116.07082	0.8382333	pos	4-Amino-2-methylenebutanoic acid	HMDB0030409	−2.1902771	−0.7244668
119	0.75_132.0656m/z	132.06558	0.7531167	pos	4-Hydroxyproline	HMDB0000725	−2.5643691	
120	0.84_175.1076m/z	175.10763	0.8382333	pos	N-Acetylornithine	HMDB0003357	−2.7493487	
121	1.13_307.0835n	308.09078	1.1279	pos	Glutathione	HMDB0000125		37.25281
122	0.86_218.0902n	219.09738	0.8552667	pos	N-gamma-L-Glutamyl-D-alanine	HMDB0036301		35.156087
123	0.77_176.1028m/z	176.10284	0.7701333	pos	Citrulline	HMDB0000904		2.4286486
124	0.74_244.0224m/z	244.02236	0.74305	neg	O-Phosphohomoserine	HMDB0003484		1.9696354
Organic nitrogen compounds								
125	15.27_124.0871m/z	124.08706	15.2738	pos	L-Histidinol	HMDB0003431	−1.4183979	−0.6265774
126	15.27_122.0966m/z	122.0966	15.2738	pos	N,N-Dimethylaniline	HMDB0001020	−1.4320285	−0.6158732
127	15.29_112.0872m/z	112.0872	15.291383	pos	Histamine	HMDB0000870	−1.4439979	−0.6506019
128	12.39_300.2895m/z	300.28947	12.385033	pos	Sphingosine	HMDB0000252		3.8095576
129	2.39_124.0395m/z	124.03947	2.3868833	pos	2-Hydroxy-4-imino-2,5-cyclohexadienone	HMDB0031713		−1.8874874
Organic oxygen compounds								
130	4.85_817.3868m/z	817.38677	4.8532667	neg	(3x,5x,10x)-9,10-Didehydroisohumbertiol O-[rhamnosyl-(1->4)-rhamnosyl-(1->2)-[rhamnosyl-(1->6)]-glucoside]	HMDB0040687	3.9229994	

Table 1. *Cont.*

No.	ID	*m/z*	Retention Time (min)	Ion Mode	Metabolites	Compound ID	PSP/PHP	FSP/FHP
131	10.96_369.2633m/z	369.26334	10.959167	pos	Mangalkanyl glucoside	HMDB0036015	3.3342658	
132	5.16_441.1765m/z	441.17651	5.15925	neg	Pteroside P	HMDB0036608	3.2783919	
133	10.14_676.3662n	699.35529	10.144617	pos	(S)-Nerolidol 3-O-[a-L-rhamnopyranosyl-(1->4)-a-L-rhamnopyranosyl-(1->6)-b-D-glucopyranoside]	HMDB0040846	3.1660281	3.0346403
134	5.16_359.1349m/z	359.13486	5.15925	neg	2′-Methoxy-3-(2,4-dihydroxyphenyl)-1,2-propanediol 4′-glucoside	HMDB0039473	1.9883008	
135	5.45_357.1192m/z	357.11919	5.4494	neg	Moringyne	HMDB0031724	1.8337359	1.9333416
136	0.76_194.0418n	193.03453	0.7600833	neg	D-Glucuronic acid	HMDB0000127	1.7667359	3.7537263
137	0.75_356.0951n	379.08431	0.7531167	pos	3-O-beta-D-Galactopyranuronosyl-D-galactose	HMDB0039726	1.7473063	
138	5.03_393.1767m/z	393.17668	5.0349167	neg	Foeniculoside IX	HMDB0033011	1.3872272	3.323785
139	5.19_463.0885m/z	463.0885	5.1942167	neg	3′-(2″-Galloylglucosyl)-phloroacetophenone	HMDB0040622	1.3004351	
140	5.36_539.1745m/z	539.17454	5.35895	neg	Torachrysone 8-(2-apiosylglucoside)	HMDB0034612	1.2716972	
141	5.18_509.2238m/z	509.2238	5.1766	neg	Linalool 3,6-oxide primeveroside	HMDB0035489	1.0205958	
142	5.14_377.1817m/z	377.18167	5.1415833	neg	7-Hydroxyterpineol 8-glucoside	HMDB0033019	0.6037439	1.8587819
143	0.76_209.0296m/z	209.02957	0.7600833	neg	Galactaric acid	HMDB0000639	0.4372531	1.7316785
144	5.14_355.1724m/z	355.17236	5.1416	pos	(1S,2S,4R)-1,8-Epoxy-p-menthan-2-ol glucoside	HMDB0033110	0.1965645	1.3746685
145	4.72_402.1525n	447.15077	4.7247833	neg	Benzyl O-[arabinofuranosyl-(1->6)-glucoside]	HMDB0041514	−0.8390669	−1.2836963
146	0.86_504.1687n	527.15791	0.8552667	pos	Gentiotriose	HMDB0029910	−1.1018444	−0.5817183
147	5.00_295.1057n	340.10362	4.99905	neg	Prunasin	HMDB0034934	−1.1644387	−3.8543421
148	9.86_329.0049m/z	329.00487	9.86165	pos	D-Sedoheptulose 7-phosphate	HMDB0001068	−1.3360925	−0.552754
149	0.79_204.0866m/z	204.08657	0.7871667	pos	N-Acetyl-D-glucosamine	HMDB0000215	−1.3540415	−0.6775015
150	0.86_522.2025m/z	522.20253	0.8552667	pos	6-Kestose	HMDB0033673	−1.4496564	−0.6952694
151	0.87_342.1158n	365.10504	0.8722833	pos	Allolactose	HMDB0038489	−1.6033747	−0.5975339
152	0.85_342.1160n	387.11424	0.8452333	neg	Trehalose	HMDB0000975	−1.6106083	
153	0.86_689.2101m/z	689.21012	0.8552667	pos	Mannan	HMDB0029931	−1.6263271	−0.6079286
154	0.84_288.0843n	289.09139	0.8382333	pos	Phlorin	HMDB0035589	−1.6994496	−0.670122
155	0.86_342.1158n	360.14975	0.8552667	pos	Inulobiose	HMDB0029898	−1.7089782	−0.7158346
156	14.21_589.4072m/z	589.40716	14.208733	pos	Lansioside C	HMDB0035103	−1.8987114	2.4629941
157	0.77_144.0655m/z	144.06547	0.7701333	pos	5-Hydroxymethyl-2-furancarboxaldehyde	HMDB0034355	−2.2634989	−1.3366433
158	0.77_164.0684n	147.06512	0.7701333	pos	2-O-Methyl-D-xylose	HMDB0033821	−3.5640663	−3.2664454
159	4.78_469.1318m/z	469.13181	4.77945	pos	4-Phenylbutyl glucosinolate	HMDB0038415		3.9823775
160	0.76_383.1000m/z	383.09996	0.7600833	neg	alpha-Hydrojuglone 4-O-b-D-glucoside	HMDB0034242		2.8118682
161	1.32_231.0838m/z	231.08378	1.3224	pos	Ethyl beta-D-glucopyranoside	HMDB0029968		2.3002148
162	0.79_315.0933m/z	315.09329	0.7941333	neg	D-erythro-L-galacto-Nonulose	HMDB0029955		1.6214985
163	0.81_479.1617m/z	479.16172	0.81115	neg	D-glycero-L-galacto-Octulose	HMDB0029954		1.4373274
164	4.35_342.1311n	365.1203	4.3501167	pos	Sphalleroside A	HMDB0032767		−1.506083
165	1.13_305.0840m/z	305.08405	1.1279	pos	Arabinopyranobiose	HMDB0029619		−1.684668
166	1.13_539.1214m/z	539.12143	1.1279	pos	b-D-Glucuronopyranosyl-(1->3)-a-D-galacturonopyranosyl-(1->2)-L-rhamnose	HMDB0039728		−2.2164514

Table 1. *Cont.*

No.	ID	*m/z*	Retention Time (min)	Ion Mode	Metabolites	Compound ID	PSP/PHP	FSP/FHP
167	2.54_360.1417n	383.13095	2.5369167	pos	2-(4-Hydroxy-3,5-dimethoxyphenyl) ethanol 4′-glucoside	HMDB0038381		−2.5423974
168	5.56_458.1789n	503.17718	5.5570667	neg	Eugenol O-[a-L-Arabinofuranosyl-(1->6)-b-D-glucopyranoside]	HMDB0037603		−3.5179227
169	4.99_295.1054n	318.09467	4.9916	pos	Sambunigrin	HMDB0034981		−4.9839447
Organohalogen compounds								
170	13.77_226.9513m/z	226.95127	13.77355	pos	Perflutren	HMDB0014696	−1.5064546	−0.654059
Organoheterocyclic compounds								
171	2.42_376.1367n	399.12588	2.424	pos	Riboflavin	HMDB0000244	−1.0930927	−2.5176871
172	0.77_118.0865m/z	118.08645	0.7701333	pos	2-Methyltetrahydrofuran-3-one	HMDB0031178	−1.231741	
173	15.17_175.1229m/z	175.12292	15.167433	pos	3-(Dimethylaminomethyl) indole	HMDB0035762	−1.4142639	−0.6390608
174	15.29_147.0916m/z	147.09158	15.291383	pos	1H-Indole-3-methanamine	HMDB0029740	−1.425459	−0.6368287
175	15.27_108.0811m/z	108.0811	15.2738	pos	6-Acetyl-1,2,3,4-tetrahydropyridine	HMDB0030345	−1.441196	−0.5951493
176	1.79_125.0235m/z	125.02348	1.7935667	pos	5-Hydroxymaltol	HMDB0032988	−1.489562	−0.594498
177	0.55_127.0390m/z	127.03905	0.5475833	pos	Maltol	HMDB0030776	−1.5004781	−0.6021647
178	0.86_163.0600m/z	163.05997	0.8552667	pos	D-1,5-Anhydrofructose	HMDB0041561	−1.7541497	−0.9841154
179	0.72_184.0732m/z	184.07321	0.7190667	pos	Tryptophanol	HMDB0003447	−2.2213504	−1.5218705
180	4.12_187.0633n	188.07057	4.12355	pos	Indoleacrylic acid	HMDB0000734	−2.3607275	−2.2746153
181	0.77_128.0474n	129.05468	0.7701333	pos	3-Hydroxy-4,5-dimethyl-2(5H)-furanone	HMDB0031306	−2.8330093	−1.9165285
182	3.87_271.1150m/z	271.11503	3.8704833	pos	Neopterin	HMDB0000845		−1.7434786
Phenylpropanoids and polyketides								
183	12.96_291.1952m/z	291.19521	12.959667	pos	Octyl 4-methoxycinnamic acid	HMDB0061861	8.2831723	
184	12.96_178.0629n	179.07014	12.959667	pos	4-Methoxycinnamic acid	HMDB0002040	4.7751364	
185	0.76_397.0791m/z	397.07908	0.7600833	neg	Decarbamoylgonyautoxin III	HMDB0040137	3.5373353	7.5091867
186	14.20_379.1561m/z	379.15614	14.2023	neg	Kanzonol M	HMDB0041101	3.014213	
187	7.26_565.2866m/z	565.28665	7.2588167	neg	Hordatine A	HMDB0030461	2.6440336	
188	14.19_357.1467m/z	357.14673	14.19105	pos	[8]-Dehydrogingerdione	HMDB0039277	2.4931618	
189	0.85_695.2246m/z	695.22456	0.8452333	neg	5-Hydroxy-7,3′,4′-trimethoxy-8-methylisoflavone 5-neohesperidoside	HMDB0030627	2.094353	
190	10.08_488.3504n	975.69367	10.076433	neg	16beta-Hydroxystellatogenin	HMDB0040391	1.6017311	
191	5.31_624.1690n	623.16171	5.305	neg	Isorhamnetin 3-O-[b-D-glucopyranosyl-(1->2)-a-L-rhamnopyranoside]	HMDB0037085	1.4061339	
192	4.46_384.1057n	383.09847	4.4620167	neg	Eleutheroside B1	HMDB0029549	1.2791289	
193	5.27_593.1512m/z	593.15122	5.2687167	neg	Kaempferol 3-neohesperidoside	HMDB0037573	1.1632915	
194	4.85_421.1637m/z	421.1637	4.8532667	neg	Mulberrin	HMDB0029507	1.0887678	
195	5.31_624.1684n	625.1757	5.3125	pos	Azaleatin 3-rutinoside	HMDB0037361	1.01554	
196	10.20_460.2690m/z	460.26903	10.204233	pos	Pectachol	HMDB0039064	−1.0181638	−0.6769391
197	9.44_432.2378m/z	432.23776	9.4353667	pos	Clausarinol	HMDB0041407	−1.127634	−0.6728349
198	1.30_164.0474n	182.08123	1.3049	pos	2-Hydroxycinnamic acid	HMDB0002641	−1.4332254	−0.6687264
199	0.92_520.1013n	543.09055	0.9234167	pos	Melitric acid B	HMDB0040680	−1.5110783	−0.5940138
200	0.86_252.0633n	253.07042	0.8552667	pos	2-O-(Z-p-Hydroxycinnamoyl)-(x)-glyceric acid	HMDB0041195	−1.7930666	−0.5375964
201	0.76_219.0449m/z	219.04493	0.7600833	neg	3-Hydroxyflavone	HMDB0031816	−3.0443569	−2.8643833
202	0.77_418.0763m/z	418.07634	0.7701333	pos	Gonyautoxin II	HMDB0033507	−6.0958687	−5.450026
203	4.23_578.1420n	579.14932	4.23295	pos	Procyanidin B1	HMDB0029754		9.5256207

Table 1. *Cont.*

No.	ID	*m/z*	Retention Time (min)	Ion Mode	Metabolites	Compound ID	PSP/PHP	FSP/FHP
204	4.24_577.1352m/z	577.13516	4.2357167	neg	Procyanidin B2	HMDB0033973		8.6781467
205	4.16_595.1465n	596.1538	4.16075	pos	3-Caffeoylpelargonidin 5-glucoside	HMDB0038087		5.5068457
206	5.95_467.1864m/z	467.18638	5.9453333	pos	Thamnosin	HMDB0030550		2.4912899
207	5.29_475.1161m/z	475.1161	5.2941167	pos	Albanin B	HMDB0034143		−1.0039232
208	5.56_571.1644m/z	571.16438	5.5570667	neg	Sakuranetin	HMDB0030090		−3.6529585

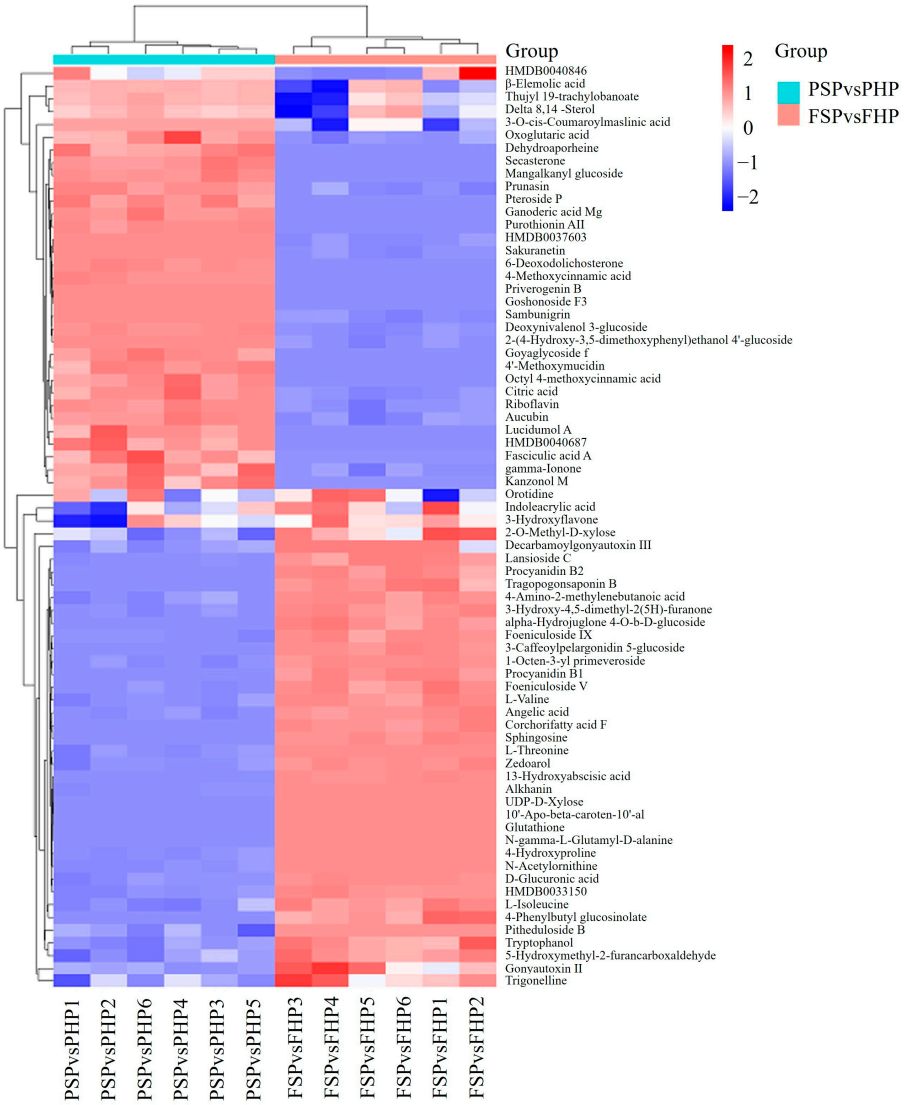

Figure 6. Top 40 differential metabolites in peach fruit before and after softening.

3.5. KEGG Annotation and Metabolic Pathway Analysis

Figure S2 shows an overview of the top 20 pathways enriched by differential metabolites in peaches before and after softening. Differential metabolite data were imported into the KEGG database to determine their position and function in related metabolic pathways. For both PSP/PHP and PTR/FHP, differential metabolites were mainly distributed in carbohydrate metabolism, amino acid metabolism, genetic information processing (aminoacyl tRNA biosynthesis and ABC transporters), and purine metabolism. In FSP/FHP, most differential metabolites were primarily involved in carbohydrate metabolism and energy production, including zeatin biosynthesis, the citrate cycle (tricarboxylic acid (TCA) cycle),

ascorbate and aldarate metabolism, pantothenate and coenzyme A (CoA) biosynthesis, nicotinate and nicotinamide metabolism, pentose and glucuronate interconversion, carbon fixation in photosynthetic organisms, glyoxylate and dicarboxylate metabolism, and amino sugar and nucleotide sugar metabolism. In PSP/PHP, most differential metabolites were mainly involved in amino acid metabolism, including arginine biosynthesis, alanine, aspartate, and glutamate metabolism, cyanoamino acid metabolism, beta-alanine metabolism, lysine biosynthesis, and arginine and proline metabolism.

4. Discussion

Fruit softening is the result of a series of complex physiological and biochemical reactions. Thus, a comparative investigation of flesh and peel before and after softening can clarify the mechanisms underlying variation in the ripening process. We observed a greater number of metabolites involved in analytical categories included in the KEGG databases in the groups PSP/PHP (i.e., peel) than in FSP/FHP (i.e., flesh). Nevertheless, considering the average flesh-to-skin weight ratio (25.5) and pit weight (8 g) of an individual experimental peach, the contribution of flesh by weight is over 25 times that of peel. Thus, the metabolic mechanism of peach flesh has an overall greater influence on fruit softening.

4.1. Degradation of Cell Wall Materials

Cell wall structural changes are generally thought to be the main factors driving fruit softening [26–28]. The distribution of cellulose is primarily observed in the primary and secondary cell walls, whereas hemicellulose forms the structural framework of the primary cell wall [29]. Furthermore, there exists a positive correlation between the contents of hemicellulose and cellulose with fruit firmness [30]. Destruction in the composition and microstructure of peach fruit cell walls during postharvest storage obviously promotes fruit softening. The cell wall hydrolases enzymatically degrade pectin, cellulose, and other polysaccharides present in the cell walls, resulting in an elevation of soluble pectin and soluble sugar content. The role of these enzymes in fruit softening has been demonstrated in various fruits such as apples [31], strawberries [32], grapes [33], and pears [34]. Our previous experiments also revealed a close relationship between polygalacturonase, β-Glucosidase, cellulase, and peach softening [11]. In this study, peach softening is accompanied by the degradation of cellulose, hemicellulose, and pectin in the cell walls of peel and flesh. We observed a significant upregulation of UDP-D-xylose and D-glucuronic acid in FSP/FHP ($|\log_2(FC)|$: 35.86 and 3.75), as well as an upregulation of UDP-glucose in FSP/FHP ($|\log_2(FC)$: 1.88). The hydrolysis of pectin produces glucuronic acid, while UDP-D-xylose is closely associated with cellulose and pectin metabolism in peaches, playing a crucial role in the metabolic pathway of amino sugars and nucleotide sugars. During this process, pectin and cellulose are degraded to form UDP-D-xylose, which is subsequently converted into UDP-glucose [35]. UDP-glucose participates in various metabolic pathways including the TCA cycle, ascorbate and aldarate metabolism, and pentose and glucuronate interconversion, thereby providing energy for storage after postharvest [35].

4.2. Energy Metabolism

The provision of energy is essential for the compounding and reinforcement of cell walls in plants. However, a limited supply of ATP and ADP declines the synthesis and fortification of cell walls, ultimately resulting in fruit softening [36,37]. The cellular energy status relies on the levels of ATP and ADP, with the TCA cycle and pentose phosphate pathway acting as primary suppliers for these metabolites. The metabolism of carbohydrates serves as the primary source of energy to meet the energy demands of fruit during storage, with amino sugar and nucleotide sugar metabolism representing key metabolic pathways, alongside starch and sucrose metabolism. However, after softening, there was a notable decrease in relevant metabolite levels within both TCA and pentose phosphate pathway in FSP/FHP and PSP/PHP, the content of related metabolites was significantly down-regulated, such as oxoglutaric acid, isocitric acid, citric acid, and D-sedoheptulose-7- phosphate, suggesting

an inadequate provision of cellular energy compared to pre-softening conditions. The study conducted by Zhang et al. (2023) demonstrates a strong association between the levels of ATP, ADP, and AMP as well as the activities of enzymes involved in energy metabolism with the inhibition of softening and maturity in jujubes [38]. Pearson's correlation tests were employed to analyze the relationship between energy metabolism and postharvest softening and quality decline in winter jujube fruits. The same phenomenon was observed in our experiments, wherein the softening process of peach fruit coincided with a deficiency in energy supply.

In cases where the supply of energy from carbohydrate metabolism is insufficient, there will be a significant upregulation in glycogenic amino acid and purine metabolism to compensate for the energy deficit. In this study, orotidine was significantly upregulated in both PSP/PHP ($|\log_2(FC)|$: 36.14) and FSP/FHP (36.16). The production of orotidine can be facilitated by D-sedoheptulose-7-phosphate, a metabolite derived from the pentose phosphate pathway, as well as through L-glutamine metabolism. Orotidine serves as a crucial intermediate in the de novo synthesis of pyrimidine nucleotides. When combined with phosphoribose, it forms uracil nucleotide (uridine monophosphate), which can further convert into other pyrimidine nucleotides and plays a role in monosaccharide transformation and polysaccharide synthesis. Purine metabolism, which is related to amino acid metabolism through the purine nucleotide cycle, plays crucial roles in energy supply, metabolic regulation, CoA production, and cellular growth [39,40].

The γ-aminobutyric acid was significantly upregulated in both FSP/FHP and PSP/PHP, primarily through three main metabolic pathways: alanine, aspartic acid, and glutamic acid metabolism; arginine and proline metabolism; and nicotinic acid and nicotinamide metabolism [41]. Alanine is metabolized via deamination to produce pyruvate, which enters glycolysis or the TCA cycle. Cellular L- aspartic acid is transaminated into oxaloacetic acid, as an important substrate for TCA cycle initiation and an important intermediate product of gluconeogenesis, it can also be metabolized to produce niacin, which is further converted into γ-aminobutyric acid [42]. Glutamic acid is deaminated into ketoglutaric acid, which enters the TCA cycle for ATP production and energy provision. Further metabolism of glutamic acid can produce γ-aminobutyric acid. L-arginine was significantly downregulated in both PSP/PHP ($|\log_2(FC)|$: 1.71) and FSP/FHP (1.34). In addition, citrulline was significantly upregulated, especially in FSP/FHP ($|\log_2(FC)|$: 2.43). Arginine is a polyamine that plays a crucial role in regulating cellular proliferation and differentiation while also modulating ion channels [42]. Arginine is metabolized mainly via decomposition into ornithine; the ornithine cycle generates urea, which is important for maintaining the cellular nitrogen metabolism balance [43].

In both PSP/PHP and FSP/FHP, the biosynthesis pathways of valine, leucine, and isoleucine were significantly downregulated. Specifically, valine and isoleucine were significantly downregulated in the softened peel, while isoleucine showed significant downregulation in the softened flesh. Acetohydroxy acid synthetase plays a crucial role in the biosynthesis pathways of valine, leucine, and isoleucine, as it catalyzes two molecules of pyruvate to produce one acetyl lactate and catalyzes one molecule of pyruvate and one molecule of butyric acid to form acetoxybutyric acid [44]. Acetyl lactate can further synthesize valine and leucine, whereas acetoxybutyric acid metabolism yields isoleucine as its final product. Acetohydroxy acid synthase is an enzyme encoded in the chloroplast nucleus that exhibits differential activity at different stages of plant development, but significantly decreased activity in aging tissues [45]. Downregulation of the biosynthesis of valine, leucine, and isoleucine indicates that softening of peach fruit is accompanied by its senescence.

4.3. Oxidative Damage

The fruit softening process is accompanied by an increase in respiratory intensity; metabolic pathways related to the respiratory chain are significantly upregulated, such as pantothenate and CoA biosynthesis, as well as nicotinate and nicotinamide metabolism.

Jiang et al. (2020) analyzed the changes in protein expression in postharvest peach fruit at different storage stages; the respiration increased, reaching a peak on day 4, at which point the fruit hardness began to show significant changes [7]. In our previous study, we detected an accumulation of reactive oxygen species (ROS), such as superoxide anion and hydrogen peroxide, during peach flesh softening [11]. The oxidative damage of cell membranes induced by ROS, which primarily occurs during respiratory metabolism, impacts fruit firmness and leads to fruit softening [46,47]. In FSP/FHP, sphingosine was significantly upregulated ($|\log_2(FC)|$: 3.81). Sphingosine is mainly derived from the degradation of sphingosine phospholipids in the cell membrane, which are important for maintaining the structure and normal function of the cell membrane [48,49]. An increase in sphingosine content in softened peaches indicates damage to the integrity of the cell membrane structure, consistent with the electron microscopy observations.

Plants can protect their cells from oxidative damage through enzymatic antioxidant defenses and non-enzymatic antioxidants [50]. Ascorbic acid-glutathione (AsA-GSH) cycle is a critical non-enzymatic antioxidant in plant cells, which removes ROS produced in the respiratory chain and maintains the cellular redox balance [50]. GSH upregulation is associated with the accumulation of superoxide anions and peroxides during fruit softening. Wang et al. (2021) showed that the oxidative damage caused by chilling injury in peaches could be reduced by regulating the ascorbic acid (AsA)–GSH cycle. Furthermore, there was a significant upregulation of glutathione (GSH) in FSP/FHP ($|\log_2(FC)|$: 37.26), primarily resulting from amino acid met down-abolism [51]. Specifically, three closely associated amino acid metabolic pathways contribute to GSH biosynthesis: alanine, aspartate, and glutamate metabolism involving the amino acids aspartate, glutamate, alanine, and γ-aminobutyric acid; arginine biosynthesis and arginine/proline metabolism encompassing the amino acids arginine, ornithine, proline, and citrulline; in addition, histidine metabolism comprising the amino acids histidine and glutamate. The metabolism of glutamate can give rise to the synthesis of glutathione. Arginine is derived from glutamic acid as a precursor, while histidine undergoes transformation via histidinase in the histidine metabolic pathway, leading to the formation of urocanic acid. Subsequently, urocanic acid is further decomposed into glutamate, which ultimately contributes to the production of glutathione.

4.4. Plant Hormone Regulation

Plant hormones are important factors in the regulation of soften and senescence of fruits, which have important effects on texture, flavor, and other quality during postharvest storage [52,53]. Trigonelline was significantly downregulated in both PSP/PHP ($|\log_2(FC)|$: 6.30) and FSP/FHP (3.41). Trigonelline is synthesized from nicotinic acid and is a plant hormone involved in the regulation of growth, development, and defense [53]; thus, the higher level before softening may support cell survival and growth, whereas after softening, cell growth is inhibited and its content decreases.

Abscisic acid (ABA) is considered to be an important substance in regulating soften and senescence of fruit. Studies have shown that ABA treatment can promote the expression of softening-related genes such as extensor protein, thus speeding up the ripening and softening process of strawberry fruit [54]. The oxidation pathway serves as the primary metabolic route for abscisic acid in numerous plant species. ABA undergoes oxidation to form hydroxyabscisic acid (HOABA), which is subsequently catalyzed into phaseic acid (PA) by enzymes. In most plants, PA does not accumulate and its 4′-keto groups are reduced to generate dihydrophaseic acid (DPA) or Epidihydrophaseic acid (epi-DPA). ABA levels increase in aging plant tissues along with the accumulation of its metabolites. Furthermore, research has demonstrated that under stress conditions, there is an intensified oxidation process in plants leading to an elevated rate of ABA metabolism and rapid buildup of metabolites such as DPA or epi-DPA [55,56]. In this study, 13-hydroxyabscisic acid (13-HOABA) was significantly upregulated in FSP/FHP ($|\log_2(FC)|$: 3.06), and epidihydrophaseic acid (epi-DPA) was significantly upregulated in both PSP/PHP ($|\log_2(FC)|$:

1.67) and FSP/FHP(|$\log_2$(FC)|: 2.52). This may be due to the accumulation of ROS that accelerates ABA oxidative metabolism. Li et al. (2023) reported that the abscisic acid content during peach soften was positively correlated with the content of most synthesis-related amino acids, suggesting a regulatory relationship between abscisic acid and amino acid metabolism [3]. In the present study, most amino acid biosynthesis pathways were downregulated, while amino acid catabolism pathways upregulated after peach fruit softening. Further studies are needed to confirm whether these changes are regulated by ABA metabolism.

Based on previous studies and our findings [3,4,7,9,11,15], we developed a model to summarize the metabolites involved in the peach fruit peel (Figure 7A) and flesh (Figure 7B) during softening.

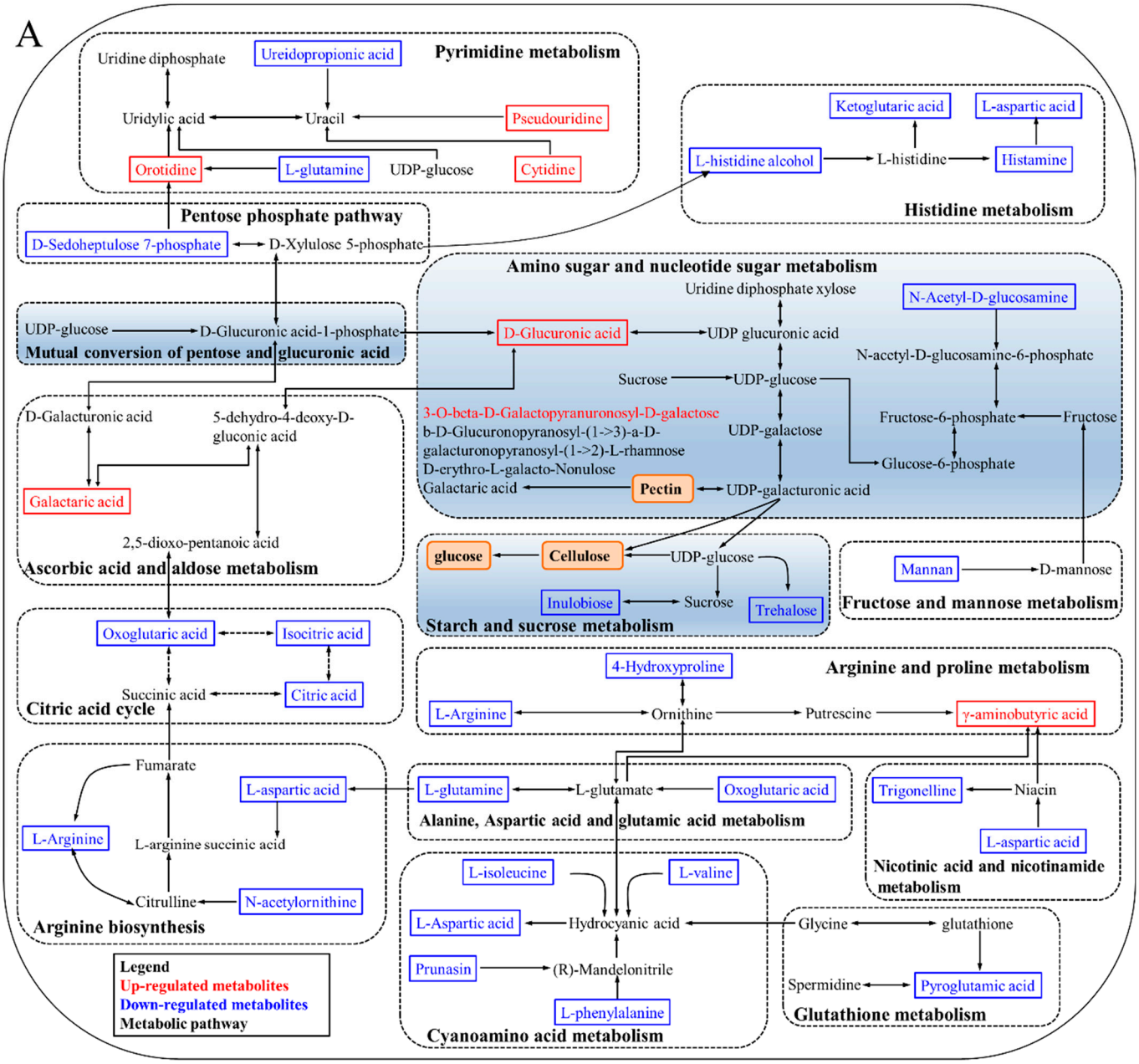

Figure 7. *Cont.*

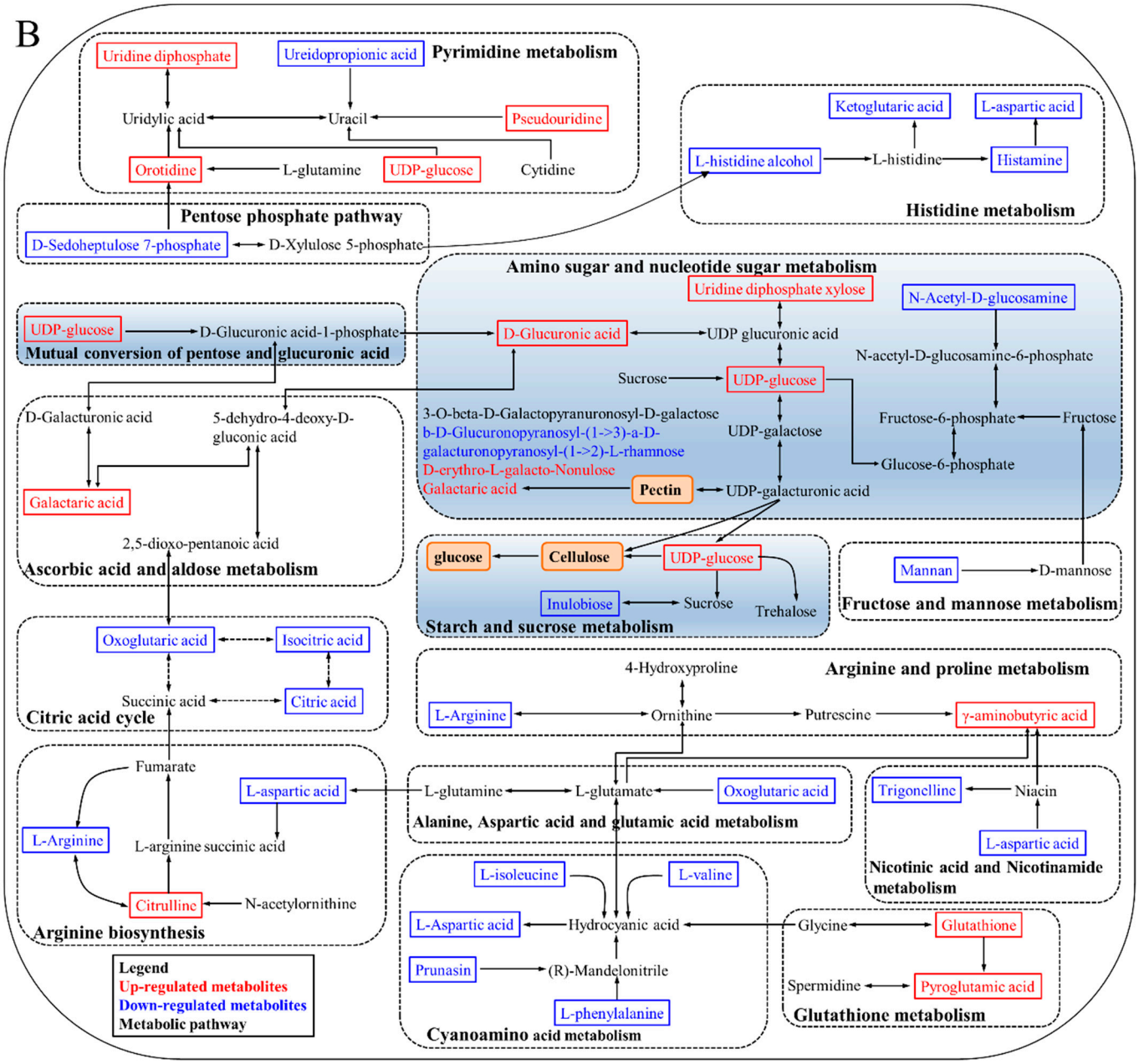

Figure 7. Metabolic pathways of the main metabolites in peel (**A**) and flesh (**B**) of peach fruit before and after softening. (Red indicates significantly up-regulated metabolites and blue significantly down-regulated metabolites in peach fresh after softening).

5. Conclusions

In this study, we investigated the mechanism of postharvest peach softening. In total, 155 and 93 significantly differential metabolites were identified from the comparative groups PSP/PHP (peel) and FSP/FHP (flesh), respectively; these metabolites included lipids, organic acids, sugars, nucleotides, phenolic acids, and flavonoids. Most were involved in carbohydrate, amino acid, purine, and energy metabolism, suggesting the involvement of these pathways in peach softening.

As a climacteric fruit, peach tissues showed a peak in respiration during storage; enhanced energy supply promoted carbohydrate metabolism, especially pectin, cellulose, and hemicellulose degradation, to provide more glycogen, and UDP-D-xylose might be one of the most key metabolites. Simultaneously, the cell walls materials were destroyed, contributing to peel and flesh softening. In cases where the supply of energy from the car-

bohydrate metabolism is insufficient, there will be a significant upregulation in glycogenic amino acid and purine metabolism to compensate for the energy deficit. The accumulation of ROS generated in the respiratory chain within cells can result in oxidative damage to cell membranes, which subsequently affects fruit firmness and leads to peach softening. At the same time, plants have the ability to safeguard their cells against oxidative damage through the utilization of antioxidants. Glutathione, a critical non-enzymatic antioxidant in plant cells, is upregulated to effectively eliminate ROS generated in the respiratory chain and maintain cellular redox homeostasis. Furthermore, plant hormones play a regulatory role in the softening process of peach fruit. Notably, the metabolism of trigonelline and abscisic acid was significantly upregulated during fruit softening.

The results of this study provide a theoretical basis for elucidating the peach softening mechanism and highlight the utility of metabolomics in mechanistic studies.

Supplementary Materials: The following supporting information can be downloaded at: https://www.mdpi.com/article/10.3390/horticulturae9111210/s1, Figure S1: Volcano plots of differential metabolites in peach fruit before and after softening. (A) PSP/PHP; (B) FSP/FHP; Figure S2. Top 20 KEGG pathway enriched by differential metabolites in peach fruit before and after softening. (A) PSP/PHP; (B) FSP/FHP.

Author Contributions: Conceptualization, X.K. and H.L. (Hong Li); methodology, investigation, Y.C., H.S., P.S. and F.Y.; data curation, H.L. (Haibo Luo); writing—original draft, X.K. and H.L. (Haibo Luo); writing—review and editing, project administration, supervision, L.Y. and H.L. (Hong Li). All authors have read and agreed to the published version of the manuscript.

Funding: This work was supported by the Innovation Guidance and Cultivation Project of Technological Innovation-based Enterprises (202204B1090016), Science and Technology Support for Mordern Agricultural Product Processing Technology of Yunnan Province, and Academician Expert Workstation in Yunnan Province (202005AF150007).

Data Availability Statement: Data are contained within the article.

Conflicts of Interest: The authors declare no conflict of interest.

References

1. Rodriguez, C.A.; Bustamante, C.A.; Budde, C.O.; Müller, G.L.; Drincovich, M.F.; Lara, M.V. Peach fruit development: A comparative proteomic study between endocarp and mesocarp at very early stages underpins the main differential biochemical processes between these tissues. *Front. Plant Sci.* **2019**, *10*, 715–734. [CrossRef]
2. Monti, L.L.; Bustamante, C.A.; Osorio, S.; Gabilondo, J.; Borsani, J.; Lauxmann, M.A.; Maulión, E.; Valentini, G.; Budde, C.O.; Fernie, A.R.; et al. Metabolic profiling of a range of peach fruit varieties reveals high metabolic diversity and commonalities and differences during ripening. *Food Chem.* **2016**, *190*, 879–888. [CrossRef] [PubMed]
3. Li, Y.; Li, L.; Zhang, X.P.; Mu, Q.; Tian, J.; Yan, J.; Guo, L.; Wang, Y.; Song, L.X.; Yu, X.Y. Differences in total phenolics, antioxidant activity and metabolic characteristics in peach fruits at different stages of ripening. *LWT-Food Sci. Technol.* **2023**, *178*, 114586. [CrossRef]
4. Kan, J.; Liu, J.; Jin, C. Changes in cell walls during fruit ripening in Chinese 'honey' peach. *J. Hortic. Sci. Biotech.* **2013**, *88*, 37–46. [CrossRef]
5. Oliveira, M.G.; Mazorra, L.M.; Souza, A.F.; Silva, G.M.C.; Correa, S.F.; Santos, W.C.; Saraiva, K.D.C.; Teixeira, A.J.; Melo, D.F.; Silva, M.G.; et al. The structure changes of water-soluble polysaccharides in papaya during ripening. *Int. J. Biol. Macromol.* **2018**, *115*, 152–156. [CrossRef]
6. Oliveira, M.G.; Mazorra, L.M.; Souza, A.F.; Silva, G.M.C.; Correa, S.F.; Santos, W.C.; Saraiva, K.D.C.; Teixeira, A.J., Jr.; Melo, D.F.; Silva, M.G.; et al. Involvement of AOX and UCP pathways in the post-harvest ripening of papaya fruits. *J. Plant Physiol.* **2015**, *189*, 42–50. [CrossRef] [PubMed]
7. Jiang, L.; Feng, L.; Zhang, F.; Luo, H.; Yu, Z. Peach fruit ripening: Proteomic comparative analyses of two cultivars with different flesh texture phenotypes at two ripening stages. *Sci. Hortic.* **2020**, *260*, 108610. [CrossRef]
8. Zhou, H.; Yu, Z.; Ye, Z. Key proteins associated to coloured compounds of peach peel using iTRAQ proteomic techniques during development and postharvest. *Sci. Hortic.* **2018**, *239*, 123–132. [CrossRef]
9. Han, S.; Cai, H.; An, X.; Huan, C.; Wu, X.; Jiang, L.; Yu, M.; Ma, R.; Yu, Z. Effect of nitric oxide on sugar metabolism in peach fruit (cv. Xiahui 6) during cold storage. *Postharvest Biol. Technol.* **2018**, *142*, 72–80. [CrossRef]
10. Huan, C.; Jiang, L.; An, X.; Yu, M.; Xu, Y.; Ma, R.; Yu, Z. Potential role of reactive oxygen species and antioxidant genes in the regulation of peach fruit development and ripening. *Plant Physiol. Biochem.* **2016**, *104*, 294–303. [CrossRef]

11. Li, X.; Peng, S.; Yu, R.; Li, P.; Zhou, C.; Qu, Y.; Li, H.; Luo, H.; Yu, L. Co-application of 1-MCP and laser microporous plastic bag packaging maintains postharvest quality and extends the shelf-life of honey peach fruit. *Foods* **2022**, *11*, 1733. [CrossRef] [PubMed]
12. Zhang, L.; Jiang, L.; Shi, Y.; Luo, H.; Kang, R.; Yu, Z. Post-harvest 1-methylcyclopropene and ethephon treatments differently modify protein profiles of peach fruit during ripening. *Food Res. Int.* **2012**, *48*, 609–619. [CrossRef]
13. Wani, A.B.; Chadar, H.; Wani, A.H.; Singh, S.; Upadhyay, N. Salicylic acid to decrease plant stress. *Environ. Chem. Lett.* **2017**, *15*, 101–123. [CrossRef]
14. Li, Z.; Xu, X.; Yang, K.; Zhu, C.; Liu, Y.; Gao, Z. Multifaceted analyses reveal carbohydrate metabolism mainly affecting the quality of postharvest bamboo shoots. *Front. Plant Sci.* **2022**, *13*, 1021161. [CrossRef]
15. Jiang, L.; Kang, R.; Feng, L.; Yu, Z.; Luo, H. iTRAQ-based quantitative proteomic analysis of peach fruit (*Prunus persica* L.) at different ripening and postharvest storage stages. *Postharvest Biol. Technol.* **2020**, *164*, 111137. [CrossRef]
16. Rajeev, K.V.; Manish, K.P.; Annapurna, C. Metabolomics in plant stress physiology. In *Plant Genetics and Molecular Biology*; Springer: Cham, Switzerland, 2018; p. 164, ISBN 978-3-319-91312-4.
17. Liu, J.; Zhang, X.; Tian, J.; Li, Y.; Liu, Q.; Chen, X.; Feng, F.; Yu, X.; Yang, C. Multiomics analysis reveals that peach gum colouring reflects plant defense responses against pathogenic fungi. *Food Chem.* **2022**, *383*, 132424. [CrossRef]
18. Johnson, C.H.; Ivanisevic, J.; Siuzdak, G. Metabolomics: Beyond biomarkers and towards mechanisms. *Nat. Rev. Mol. Cell Biol.* **2016**, *17*, 451–459. [CrossRef]
19. Dai, J.Y.; Xu, Z.; Xu, Y.T.; Fang, Z.H.; Shah, K.; Kang, T.Y.; Wu, H.X.; Zhang, D.; Xing, L.B.; Ma, J.J.; et al. A novel NAC transcription factor, PpNAP6, is involved in peach ripening by activating ethylene synthesis. *Postharvest Biol. Technol.* **2023**, *201*, 112363. [CrossRef]
20. Sun, H.; Wang, H.; Zhang, A.; Yan, G.; Zhang, Y.; An, N.; Wang, X. Berberine ameliorates nonbacterial prostatitis via multi-target metabolic network regulation. *OMICS* **2015**, *19*, 186–195. [CrossRef]
21. Zhang, M.; Li, Y.; Mu, Q.; Feng, F.; Yu, X.; Ge, J.; Zhang, Y.; Nie, J. Effects of chlorpyrifos on the metabolic profiling of Bacillus megaterium strain RRB. *Chemosphere* **2022**, *297*, 134189. [CrossRef]
22. Fonseca, T.A.H.; Von, R.C.P.; Araújo, R.; Oliveira, M.C.; Justino, G.C.; Bento, L.; Calado, C.R.C. The impact of the serum extraction protocol on metabolomic profiling ysing UPLC-MS/MS and FTIR spectroscopy. *ACS Omega* **2023**, *8*, 20755–20766. [CrossRef] [PubMed]
23. Emmanuel, A.; Yu, Y.; Chen, C.S.; Lu, L.; Hu, S.K.; Yu, H.P.; Ma, Q.Q.; Kuberan, T.; Rajiv, P.; Anburaj, J.; et al. Untargeted metabolomic analysis using UPLC-MS/MS identifies metabolites involved in shoot growth and development in pruned tea plants (*Camellia sinensis* (L.) O. Kuntz). *Sci. Hortic.* **2020**, *264*, 109164. [CrossRef]
24. Luo, H.; Zhou, T.; Kong, X.; Tao, M.; Zhang, J.; Wang, W.; Jiang, L.; Yu, L.; Yu, Z. iTRAQ-based mitochondrial proteome analysis of the molecular mechanisms underlying postharvest senescence in *Zizania latifolia*. *J. Food Biochem.* **2019**, *43*, e13053. [CrossRef] [PubMed]
25. Shi, J.; Xia, C.; Tian, Q.; Zeng, X.; Wu, Z.; Guo, Y.; Pan, D. Untargeted metabolomics based on LC-MS to elucidate the mechanism underlying nitrite degradation by *Limosilactobacillus fermentum* RC4. *LWT-Food Sci. Technol.* **2022**, *163*, 113414. [CrossRef]
26. Fabrizio, C.; Luca, C.; Marco, F.; Sara, L.; Walter, G.; Pierluigi, M.; Flavia, G.; Franco, B. Texture dynamics during postharvest cold storage ripening in apple (Malus × domestica Borkh.). *Postharvest Biol. Technol.* **2012**, *69*, 54–63. [CrossRef]
27. Wang, S.Y.; Zhou, Q.; Zhou, X.; Zhang, F.; Ji, S.J. Ethylene plays an important role in the softening and sucrose metabolism of blueberries postharvest. *Food Chem.* **2020**, *310*, 125965. [CrossRef]
28. Liu, B.; Wang, K.; Shu, X.; Liang, J.; Fan, X.; Sun, L. Changes in fruit firmness, quality traits and cell wall constituents of two highbush blueberries (*Vaccinium corymbosum* L.) during postharvest cold storage. *Sci. Hortic.* **2019**, *246*, 557–562. [CrossRef]
29. Zhang, Q.; Tang, F.; Cai, W.; Peng, B.; Ning, M.; Shan, C.; Yang, X. Chitosan treatment reduces softening and chilling injury in cold-stored Hami melon by regulating starch and sucrose metabolism. *Front. Plant Sci.* **2022**, *13*, 1096017. [CrossRef]
30. Chen, Y.; Zhu, C.C.; Zhao, Y.Q.; Zhang, S.J.; Wang, W. Transcriptomics integrated with changes in cell wall material of chestnut (*Castanea mollissima* Blume) during storage provides a new insight into the "calcification" process. *Foods* **2022**, *11*, 1136. [CrossRef]
31. Favre, L.; Hunter, D.A.; Erridge, Z.A.; Napier, N.J.; Punter, M.; Carr, B.; Tattersall, A.; Johnston, J.W.; Heyes, J.A.; Lill, R.E.; et al. Seasonal differences in softening of early-harvested 'Royal Gala' apple fruit are correlated with at-harvest biomarkers indicative of abiotic stress responses. *Postharvest Biol. Technol.* **2023**, *195*, 112131. [CrossRef]
32. Ivan, O.D.; Irene, R.; Dolores, M.A.; Tarradas, R.; Sanchez-Ballesta, M.T.; Escribano, M.I.; Merodio, C. Transcriptomic analysis of CO_2-treated strawberries (*Fragaria vesca*) with enhanced resistance to softening and oxidative stress at consumption. *Front. Plant Sci.* **2022**, *13*, 983976. [CrossRef]
33. Coletta, C.; Botondi, R.; Forniti, R.; Baccelloni, S.; Bellincontro, A.; Mencarelli, F. Alternating temperature in postharvest cooling treatment of 'Fiano' and 'Falanghina' grapes affects cell wall enzyme rate, berry softening and polyphenols. *J. Sci. Food Agric.* **2018**, *99*, 3142–3148. [CrossRef]
34. Xiang, F.X.; Gao, R.; Chen, Y.; Pang, J.W.; Liu, S.S.; Tian, L.; Zhai, R.; Wang, Z.G.; Xu, L.F. Exogenous putrescine and 1-methylcyclopropene prevent soft scald in 'Starkrimson' pear. *Postharvest Biol. Technol.* **2022**, *193*, 112035. [CrossRef]
35. Yao, S.; Cao, Q.; Xie, J.; Deng, L.; Zeng, K. Alteration of sugar and organic acid metabolism in postharvest granulation of Ponkan fruit revealed by transcriptome profiling. *Postharvest Biol. Technol.* **2018**, *139*, 2–11. [CrossRef]

36. Li, D.; Li, L.; Xu, Y.Q.; Wang, L.; Lin, X.Y.; Wang, Y.S.; Luo, Z. Exogenous ATP attenuated fermentative metabolism in postharvest strawberry fruit under elevated CO_2 atmosphere by maintaining energy status. *Postharvest Biol. Technol.* **2021**, *182*, 111701. [CrossRef]
37. Aghdam, M.S.; Jannatizadeh, A.; Luo, Z.; Paliyath, G. Ensuring sufficient intracellular ATP supplying and friendly extracellular ATP signaling attenuates stresses, delays senescence and maintains quality in horticultural crops during postharvest life. *Trends Food Sci. Technol.* **2018**, *78*, 67–81. [CrossRef]
38. Zhang, J.; Wang, C.; Chen, C.; Zhang, S.; Zhao, X.; Wu, C.; Kou, X.; Xue, Z. Glycine betaine inhibits postharvest softening and quality decline of winter jujube fruit by regulating energy and antioxidant metabolism. *Food Chem.* **2023**, *410*, 135445. [CrossRef]
39. Chen, H.; Lai, X.; Wang, L.; Li, X.; Chen, W.; Zhu, X.; Song, Z. Ethylene response factor MaERF012 modulates fruit ripening by regulating chlorophyll degradation and softening in banana. *Foods* **2022**, *11*, 3882. [CrossRef]
40. Shan, Y.; Li, F.; Lian, Q.; Xie, L.; Zhu, H.; Li, T.; Zhang, J.; Duan, X.; Jiang, Y. Role of apyrase-mediated eATP signal in chilling injury of postharvest banana fruit during storage. *Postharvest Biol. Technol.* **2022**, *187*, 111874. [CrossRef]
41. Zhang, Y.; Guo, Y.; Song, X. Comprehensive insight into an amino acid metabolic network in postharvest horticultural products: A review. *J. Sci. Food Agric.* **2023**, *103*, 5667–5676. [CrossRef]
42. Lefèvre, P.L.C.; Palin, M.F.; Murphy, B.D. Polyamines on the reproductive landscape. *Endocr. Rev.* **2011**, *32*, 694–712. [CrossRef] [PubMed]
43. Kesarwani, P.; Kant, S.; Prabhu, A.; Chinnaiyan, P. The interplay between metabolic remodeling and immune regulation in glioblastoma. *Neuro-Oncology* **2017**, *19*, 1308–1315. [CrossRef] [PubMed]
44. Shao, S.N.; Li, B.; Sun, Q.; Guo, P.R.; Du, Y.J.; Huang, J.F. Acetolactate synthases regulatory subunit and catalytic subunit genes VdILVs are involved in BCAA biosynthesis, microscletotial and conidial formation and virulence in Verticillium dahlia. *Fungal Genet. Biol.* **2022**, *159*, 103667. [CrossRef] [PubMed]
45. Wang, C.W.; Dissing, M.M.; Agerbirk, N.; Crocoll, C.; Halkier, B.A. Characterization of Arabidopsis CYP79C1 and CYP79C2 by glucosinolate pathway engineering in *Nicotiana benthamiana* shows substrate specificity toward a range of aliphatic and aromatic amino acids. *Front. Plant Sci.* **2020**, *11*, 57–64. [CrossRef] [PubMed]
46. Kan, J.; Wang, H.M.; Jin, C.H.; Xie, H. Changes of reactive oxygen species and related enzymes in mitochondria respiratory metabolism during the ripening of peach fruit. *Agric. Sci. China* **2010**, *9*, 138–146. [CrossRef]
47. Meitha, K.; Pramesti, Y.; Suhandono, S. Reactive oxygen species and antioxidants in postharvest vegetables and fruits. *Int. J. Food Sci.* **2020**, *2020*, 8817778. [CrossRef]
48. Diaz, E.R.; McCullough, L.D.; Tsvetkov, A.S. The functional role of sphingosine kinase 2. *Front. Mol. Biosci.* **2021**, *8*, 683767. [CrossRef]
49. Toshikazu, H.; Toshihiko, S.; Shigeo, K.; Takamitsu, S.; Takayuki, K.; Yasuyuki, I. Synthesis of fluorescence-Labeled sphingosine and sphingosine 1-phosphate; effective tools for sphingosine and sphingosine 1-phosphate behavior. *Bioorg. Med. Chem. Lett.* **2003**, *13*, 661–664. [CrossRef]
50. Dong, B.; Yao, Q.; Zhu, D.; Han, H.; Tang, H.; Ding, X. Exogenous melatonin maintains quality of postharvest *Rosa roxburghii* fruitby modulating reactive oxygen species metabolism and energy status. *Sci. Hortic.* **2022**, *304*, 111346. [CrossRef]
51. Wang, C.; Huang, D.; Tian, W.; Zhu, S. Nitric oxide alleviates mitochondrial oxidative damage and maintains mitochondrial functions in peach fruit during cold storage. *Sci. Hortic.* **2021**, *287*, 110249. [CrossRef]
52. Romero, I.; Escribano, M.I.; Merodio, C.; Sanchez, B.M.T. Postharvest high-CO_2 treatments on the quality of soft fruit berries: An integrated transcriptomic, proteomic, and metabolomic approach. *J. Agric. Food Chem.* **2022**, *70*, 8593–8597. [CrossRef] [PubMed]
53. Delphine, M.P.; Vallarino, J.G.; Osorio, S. Review: Metabolite changes during postharvest storage: Effects on fruit quality traits. *Metabolites* **2020**, *187*, 10050187. [CrossRef]
54. Springsteen, G.; Yerabolu, J.R.; Nelson, J.; Rhea, C.J.; Krishnamurthy, R. Linked cycles of oxidative decarboxylation of glyoxylate as protometabolic analogs of the citric acid cycle. *Nat. Commun.* **2018**, *9*, 91–100. [CrossRef]
55. Alves, V.E. Exogenous abscisic acid (ABA) and jasmonate (JA) promote metabolic regulation in Jacarandá-Pardo (*Machaerium villosum* Vog.) seedlings under PEG-induced water deficit. *Plant Stress* **2023**, *9*, 100174. [CrossRef]
56. Elisabeth, P.; Olivier, R.; Claudie, R.; Stéphanie, B.M.; Alessandra, M.G.; Limami, A.M. Nitrogen metabolism responses to water deficit act through both abscisic acid (ABA)-dependent and independent pathways in Medicago truncatula during post-germination. *J. Exp. Bot.* **2011**, *62*, 605–615. [CrossRef]